



Article

# On the Role of LiF in Organic Optoelectronics

Ayse Turak

Department of Engineering Physics, McMaster University, 1280 Main St. W, Hamilton, ON L8S 4L7, Canada; turaka@mcmaster.ca; Tel.: +1-905-525-9140 (ext. 23348)

**Abstract:** Organic optoelectronic device behaviour is heavily dependent on interfacial effects due to the device architecture and thickness. Interfaces between the inorganic electrodes and the active organic layers play a defining role in the all of the electronic and stability processes that occur in organic light emitting diodes (OLEDs) and organic solar cells (OPVs). Amongst the many interlayers introduced at these interfaces to improve charge carrier movement and stability, LiF has proven to be the most successful and it is almost ubiquitous in all organic semiconductor devices. Implemented at both top and bottom contact interfaces, doped into the charge transporting layers, and used as encapsulants, LiF has played major roles in device performance and lifetime. This review highlights the use of LiF at both top and bottom contacts in organic optoelectronics, discusses the various mechanisms proposed for the utility of LiF at each interface, and explores its impact on device lifetimes. From examples relating to charge carrier flow, interfacial electronic level modification, and interfacial stability, a comprehensive picture of the role of LiF in organic devices can be formed. This review begins with a brief overview of the role of the interface in OLEDs and OPVs, and the general properties of LiF. Then, it discusses the implementation of LiF at the top contact electrode interface, followed by the bottom substrate contact electrode, examining both performance and degradation effects in both cases.

**Keywords:** interlayers; OLEDs; OPVs; stability; performance; nanoparticles



**Citation:** Turak, A. On the Role of LiF in Organic Optoelectronics. *Electron. Mater.* **2021**, *2*, 198–221. <https://doi.org/10.3390/electronicmat2020016>

Academic Editor: Roberto Centore

Received: 17 April 2021  
Accepted: 25 May 2021  
Published: 3 June 2021

**Publisher's Note:** MDPI stays neutral with regard to jurisdictional claims in published maps and institutional affiliations.



**Copyright:** © 2021 by the author. Licensee MDPI, Basel, Switzerland. This article is an open access article distributed under the terms and conditions of the Creative Commons Attribution (CC BY) license (<https://creativecommons.org/licenses/by/4.0/>).

## 1. Introduction

Semiconducting devices utilizing  $\pi$ -conjugated organic molecules have been of significant research interest for over 30 years, with next generation hardware systems based on organic light emitting diodes (OLED), organic photovoltaics (OPV), organic transistors, organic memory devices, and organic sensors all being developed and optimized. OLEDs are already available commercially in lighting and displays [1], and organic photovoltaics (OPVs) have reached efficiencies surpassing amorphous silicon, and approaching thin film crystalline Si solar cells [2,3].

In all such molecular devices, heterojunctions between electrodes, interlayers, and active materials play a strategic role. For OLEDs, effective carrier injection and light extraction are managed by the interfacial structures between the organic active layers and the inorganic contacts. For OPVs, all of the major processes are defined by the nature of heterojunctions: organic/organic interfaces determine the exciton separation efficiency; organic/inorganic interfaces with substrates determine the active layer morphology, which critically determines charge transport; and electrode/active layer junctions dictate charge extraction efficiency. Similarly, the long term viability of organic devices is dependent on minimizing interfacial electronic level modifications, interfacial chemical reactions, and interfacial morphological changes.

Lithium fluoride (LiF) is widely used as a buffer layer in organic devices, even though as a wide band gap insulator, it should have inaccessible energy levels. The introduction of LiF in organic devices has been shown to modify electrode work function [4–7], modify the interfacial reactivity [8–10], and modify the contact adhesion [11,12]. This has allowed LiF to be effectively implemented at both top and bottom electrodes to improve device

performance. Additionally, LiF interlayers also have significant impacts on the stability of organic devices, through control of interfacial chemical interactions and modifications of the interface morphology at either electrode.

In this contribution, the aim is to highlight the use of LiF in organic optoelectronic devices to understand its impact on performance and stability. From examples of our own research and others relating to electrical behaviour, interfacial chemical interactions, and interfacial morphological changes, a comprehensive picture of the role that LiF plays at interfaces in devices can be made.

## 2. Role of the Interface in Organic Devices

Organic optoelectronic devices are most commonly used in diode configurations, consisting of a multilayer structure built up on a glass substrate, with the active organic films sandwiched between two dissimilar electrodes, as developed by Kodak in the late 1980's [13,14]. For typical device configurations, the bottom contact is deposited first, directly onto the substrate. Such contacts tend to be thin transparent conductive films of high work function suitable for hole injection (typically indium tin oxide (ITO)), with additional electrode materials for inverted configurations. Atop the electrode, one or more organic layers are deposited, each between 50 and 100 nm, that can act as hole-injecting, hole transporting, light emitting or absorbing, electron transporting and electron injection/hole blocking layers. The top contact is then evaporated or screen printed on top of these organic layers. Multiple evaporation/deposition steps may be required for electrode formation if multilayer electrodes are desired. Finally, the device is usually encapsulated to prevent oxidation of the various layers.

The thickness of these devices, generally between 0.1 and 2.2  $\mu\text{m}$ , magnifies the role of the interface in device behaviour, as the interfacial interaction region can dominate the thickness of the active layers. The major effect of the interfacial properties is on carrier injection, and therefore on effective conduction, absorption, and luminescence, and on long term device reliability.

### 2.1. Carrier Motion across Electrode Interfaces

Due to the observed temperature dependence of the current–voltage behaviour of organic devices, electron injection into or charge extraction out of the organic layer is presumed to be controlled mainly by a thermionic emission process, governed by a modified Richardson Equation [15]

$$J_{inj} = 4\zeta^2 N_o e \mu E \exp\left(\frac{-\phi_B}{kT}\right) \exp\left(\left(\frac{e^3 E}{4\pi\epsilon(kT)^2}\right)^{1/2}\right) \quad (1)$$

where  $\zeta$  is a function of the electric field,  $N_o$  is the density of charge hopping sites,  $\phi_B$  is the barrier to injection,  $E$  is the applied electric field strength,  $\mu$  is the electron mobility,  $\epsilon$  is the material permittivity and  $e$  is the electron charge.

Most of the variables controlling this mechanism are set either by the device conditions, such as the applied electric field and operating temperature, or by the organic layer properties, such as the dielectric constant, thickness or mobility. Therefore, it is the interfacial conditions—the barrier to charge injection and the density of interfacial sites—that control the modification of injection properties. Baldo et al. [16] has shown that the barrier to charge injection is controlled by the formation of interface dipoles, with injection from this dipole region into the organic being the limiting mechanism. This is supported by experimental evidence of band bending and Fermi level pinning, showing that the organic molecular orbital-metal Fermi energy band offset was independent of the metal work function for various organic materials [17–19]. Other effects such as the “pillow” or “push-back” effect [20,21], the integer charge transfer model [22,23], induced density of interface states (IDIS) model [23–25], interfacial electrostatics model [26], metal induced gap

states [27–30] and tunnelling barriers [30,31], which have also been proposed as possible injection mechanisms, are also confined to the interfacial region.

## 2.2. Device Reliability

Unlike inorganic optoelectronic systems, all organic devices are prone to instability, with performance degrading over timescales that can affect large scale commercialization [32]. As efficiencies continue to increase, device lifetime is the second critical parameter for organic device commercialization [12,33,34]. Contrary to their inorganic counterparts, organic semiconductor devices are not intrinsically stable chemically or insensitive to light and the ambient environment. Rather the small molecule or polymer active layers themselves, the electrodes, and all interfaces are all susceptible to degradation. Consequently, no single mechanism can completely describe the complex processes involved in degradation in organic devices.

Occurring during operation and storage, degradation for organic systems is a continuous process, taking three forms: loss of conjugation of the active layers and irreversible deterioration, loss of the conductive properties at interfaces, and mechanical disintegration [12]. Degradation mechanisms are known to include crystallization or oxidation of organic layers, electrode oxidation, interfacial reactions between various components, diffusion of electrode and interlayer materials, diffusion of molecular oxygen and water into the device, intermixing and interdiffusion of organic materials, phase segregation and dewetting, delamination of any layer, and the formation of bubbles, debris and cracks [12,34,35]. All result in loss of the measured electrical properties. It is common to describe the device lifetime using the time it takes to decay as some percentage of the initial performance, typically 50% or 80% of initial performance for OLEDs ( $t_{50}$ ) and OPVs ( $t_{80}$ ), respectively.

Both top and bottom contacts are vectors of instability in organic devices. The top metal contact is typically the most vulnerable, as degradation there proceeds more rapidly than anywhere else in the device [34]. The possibility of chemical reactions that can take place at the interface, such as the destructive reaction of the organic layer induced by the electrode [36,37], or the electrochemical coupling of cathode alloy components [38], can greatly affect both the long and short term device characteristics. Additionally, the surface morphology and interfacial defects can act to limit device performance through cathode delamination [12,38,39], or pinhole formation [40,41], which are often linked to interfacial reactions. Delamination for OLEDs and OPVs, exaggerated for flexible devices, could result from oxide formation yielding interfacial volume changes [42], hygroscopic interlayers at inorganic electrodes, such as PEDOT:PSS or LiF [11,43] swelling or dissolving with exposure to ambient water; or active organic layers swelling with water or solvent vapour absorption [44]. Top contact delamination results from a cohesive failure within the organic layer, with the fracture plane roughly within 5–10 Å of the interface [12,37,45], outside of any interfacial interaction zone.

As the substrate upon which the device is built, the bottom contact is also influential in device stability. Morphological, chemical and electronic changes over the lifetime of the device all contribute to device failure [34]. There are four criteria which result in an unstable interface: a mismatch in surface energy, a material with low glass transition temperature, a reaction between organic and substrate materials, and an inconsistent surface work function. An erratic and mutable interface is detrimental to both OLEDs and OPVs as the device response critically depends on the nature of the electrode interface and of the hole transporting (electron donating) (HTL) film deposited on it [34].

## 3. LiF General Properties

Lithium fluoride (LiF) is an alkali halide that appears as a solid white powder. It forms as an ionic crystal with the cubic rock salt (NaCl) structure, occurring in nature as griceite, an extremely rare mineralogical form [46]. With a bulk lattice parameter of 4.0271 Å [47], lithium and fluorine in LiF have the smallest radius between alkali and halide ions. The Li–F bond distance (i.e., nearest neighbour distance) in face centred cubic (FCC)-solid LiF

is 2.014 Å while the cation-anion bond length  $R_0$  in the isolated molecule is 1.586 Å [48]. This is a result of fluorine having the highest electron affinity amongst all the elements. LiF monomers have high dipole moments of 6.3 Debye, giving it a strongly ionic character.

The special technological and scientific interest in LiF stems from its electrical and optical properties. Due to its high band gap of 13.6 eV [49], one of the largest known for solids, LiF makes an excellent electrical insulator, and is useful for specialized optics in the ultraviolet region of the electromagnetic spectrum [50–52]. However, ultrathin layers of thermally evaporated LiF are known to reduce the work function of metal electrodes, significantly enhancing carrier injection and field emission in semiconductor devices [5]. LiF produced from solution [6,7] has been used to tune the ITO surface work function, using surface dipoles. Dipole layers in LiF thin films on diamond surfaces have also been seen to lower the surface work function by inducing negative electron affinity [53].

LiF is particularly susceptible to irradiation and heating, developing optically and electrically active defects, colour centres, and hardening sites [54–57]. LiF is unique in that any kind of ionizing radiation can create defects that are room temperature stable [56]. This ability to form stable active defects makes LiF particularly attractive for applications in optoelectronics [55].

Thin films of LiF are mainly produced by vapor deposition techniques, with LiF sublimating at 845 °C [58]. Evaporative deposition of LiF is generally substrate independent for amorphous and polycrystalline substrates [59,60], including ITO [61], and organic surfaces [62]. When thermally evaporated, LiF has a granular and porous morphology, with large surface roughness [57,61,63], being made up of crystallites roughly an order of magnitude larger than the nominal deposited thickness [61,62]. This is thought to result from the strong ionic bonding in LiF preventing full wetting of thin layers on the surface [59,60,64]. However, the size of crystallites can greatly depend on the deposition conditions. Slower deposition rates, at lower evaporation temperatures, can result in significantly smaller island sizes than those formed at higher deposition rates [61] due to the higher prevalence of monomer evaporation as evaporation temperature decreases [65,66]. A deposition greater than 3 nm, as measured by a quartz crystal thickness monitor (QCM), is typically needed to form complete layers on most surfaces [59,61,64,67,68]. At 1 nm deposition, as measured by QCM, coverage is ~80%; below this nominal thickness, crystallites of roughly the same size cover less and less area [61,62]. The vapour phase of LiF tends to consist of dimers, trimers and higher order LiF clusters during evaporation [65,66,69–71], resulting in roughly similar sized islands of LiF nanoparticles coalescing on the surface until a full layer is formed.

Structurally, LiF thin films are similar to their bulk crystallographic structures, with a polycrystalline arrangement where the (111) planes are nearly normal to low temperature substrate surfaces ( $T_s < 200$  °C) [64] ( $\langle 1697 \rangle$  surface texture [68]). At higher substrate temperatures during growth ( $T_s \geq 250$  °C), crystallites are arranged with their  $\langle 100 \rangle$  orientation parallel to the substrate surface ( $\langle 522 \rangle$  surface texture [68]). Deposition at high substrate temperatures ( $T_s$  greater than 300 °C) results in fully oriented single crystals rather than polycrystalline films [72,73].

To take advantage of fully solution processed organic devices and controllable sub-monolayer coverage of LiF, Turak and coworkers [6,7,61,74] produced uniform LiF nanoparticles from diblock copolymer micelle templates. Using reverse micelles not only results in the formation of particles with a very narrow size distribution of less than 2% variation in the particle diameters [7,74], but also allows the monolayer deposition of LiF nanoparticles with less than 15% surface coverage. Surface coverage by mostly disconnected LiF islands can be systematically increased using successive coating and etching steps until a complete layer is formed [6,7,61].

#### 4. LiF Interlayers at Top Contact Interfaces

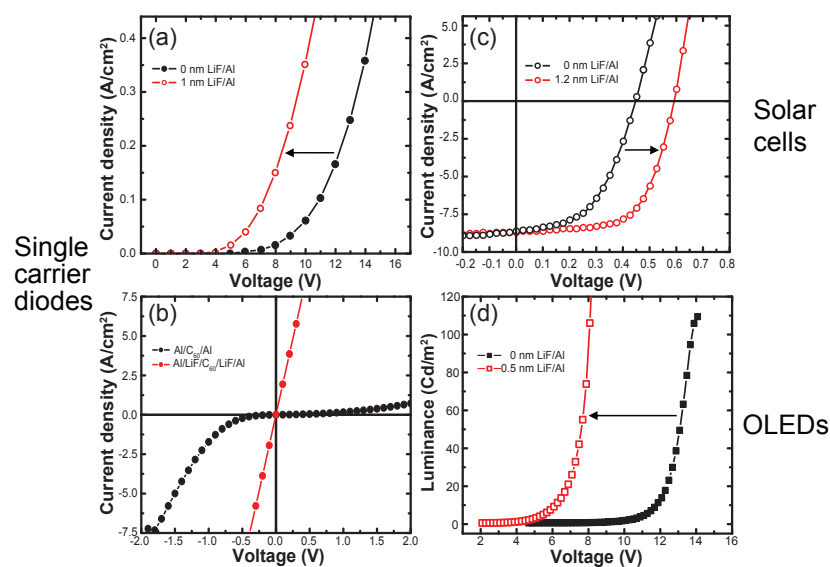
Historically, with limited understanding of the true nature of organic/metal interfaces, the barrier to charge injection was presumed to simply be the difference between the lowest

unoccupied molecular orbital (LUMO) of the organic molecule and the work function of the metal cathode in contact. Therefore, initial studies used low work function metals as the top contact, including Li, Mg, and Ca [75]. Such low work function cathodes, which achieve high injection efficiency due to the ease of electron stripping, are unfortunately also highly reactive and unstable. Therefore, they are prone to oxidative or corrosive attack by the organic layers or by atmospheric gases [12,34].

As well, due to the small size and relatively high thermal energy of the evaporated metal, the impinging "hot" atoms can diffuse into the weakly bonded organic layers [76–79]. This can severely limit their injection behaviour, such as the case of metal diffusion from Ca cathodes leading to photoluminescence quenching in oligomers [80], or the formation of recombination centres in P3HT:PCBM [81].

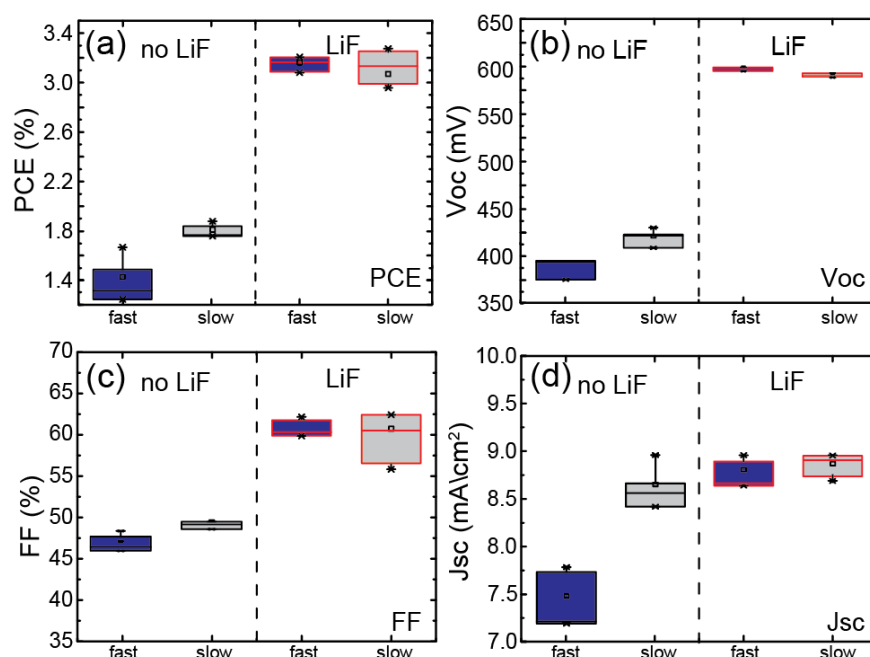
To mitigate these effects, attempts were made to modify the cathode materials by alloying with more stable metals or by introducing interfacial buffer layers. The shift to multilayer electrodes also led to the adoption of more stable metals, such as Al and Ag, which generally showed poor injection characteristics by themselves. In 1997, Jabbour et al. [82] and Hung et al. [19], within months of each other, introduced a LiF interlayer for a device based on an Alq<sub>3</sub> electron transport (ETL) and emitting layer (EML), and the bilayer Al/LiF electrode has been the most ubiquitous and effective top contact electrode for most organic devices, due to its superior properties and ease of reproducible fabrication compared to alloy cathodes.

Figure 1 shows the impact of introducing a LiF interlayer beneath an Al top contact electrode for single carrier devices, OLEDs and solar cells. For single carrier diodes, it can significantly reduce the built-in voltage, achieving a flat band condition at much lower injecting voltages and producing ohmic contacts. For OPVs, the open circuit voltage is significantly increased, leading to higher conversion efficiencies. For OLEDs, both current density and luminance are significantly increased, with a lower turn-on voltage. For all cases, the introduction of LiF has improved the device performance.



**Figure 1.** (a) Impact of a thin LiF layer (1.0 nm) between cathode metal and electron transport material on the current–voltage, I–V, characteristics for Alq<sub>3</sub> (65 nm). Insertion of LiF between aluminum and Alq<sub>3</sub> significantly enhances the injection current. Adapted from Ref. [83] copyright (2000) with permission from Elsevier. (b) I–V characteristics of Al/C<sub>60</sub>/Al devices with and without LiF interlayer 0.5 nm. The bias was applied to the bottom electrode in reference to the top grounding electrode. Adapted from Ref. [84] with the permission of AIP Publishing. (c) Typical illuminated current density–voltage, J–V, curves for photovoltaic cells with the inclusion of a LiF layer. Adapted from Ref. [85] with the permission of AIP Publishing. (d) Luminance–voltage (L–V) characteristics of multilayer OLED device with Alq<sub>3</sub> electron transporting layer. Device structure glass/ITO/NPB(60 nm)/Alq(25 nm)/LiF (0 or 0.5 nm)/Al(150 nm).

The effectiveness of LiF in improving charge motion at the interface is highlighted by a study of the impact of solvent annealing in P3HT:PCBM based solar cells [85], where the LiF interlayer overshadows the impact of other processing steps and even accommodates suboptimal morphology development. In that study, Turak et al. [85] showed that introducing a LiF interlayer almost eliminates the need to optimize growth and annealing parameters, with both solvent annealed (“slow”) and non-solvent annealed (“fast”) films having much improved and similar device properties, as shown in Figure 2. Without the LiF interlayer, not only did the devices perform much worse, but the drying time had a significant affect on the device performance. This underscores the importance of the interface in such devices.



**Figure 2.** Box plots for the (a) power conversion efficiency, (b) open circuit voltage, (c) fill factor, and (d) short-circuit current, for fast and slow drying of P3HT:PCBM solar cell films, with and without a LiF interlayer. Data incorporate results from 10 devices. Adapted from Ref. [85] with the permission of AIP Publishing.

While the positive influence of LiF on device efficiency is well documented [4,19,84,86–88], the underlying working principle is still somewhat controversial. It is generally understood that Al/LiF forms a “good” contact, with dramatically enhanced energy-level alignment with a number of organic materials, resulting in ohmic or quasi-ohmic behaviour [84,89,90].

Changing the electrode metal or organic transport layers has a major influence on the effectiveness of a thin LiF interlayer, with certain bilayer combinations, such as Mg/LiF [10,83,91] having a negative effect on device performance, while others such as Ag/LiF [31,92] have no effect at all for small molecule or fullerene based ETLs (see Figure 3). For polymeric conducting layers, other bilayer combinations such as CsF/Al and LiF/Ca/Al, are more effective electrodes [93,94].

The many investigations into the impact of an interlayer between the organic and the metal cathode have resulted in the proposal of many conflicting mechanisms, for all of which there is both supporting and contradicting evidence. These mechanisms include electron tunnelling through thin insulator layers [19,87], band bending at the metal/organic interface [19,87], lowering of the cathode metal work function [4,5], introducing interfacial dipoles [16], and doping of the organic layer with ions dissociated from the interfacial compound [95–97]. Due to the strong bonding of LiF, dissociation was speculated to require the presence of Al and moisture [95,98]. Though it is widely believed that LiF dissociation is the dominant mechanism [31,95,99,100], there has been no conclusive evidence of the

strong ionic bonding of LiF being broken [8,9,91] nor of Li and F existing in a chemical state other than LiF [9,19,87,95,100,101], though charge transfer between the LiF and organic layers are often observed [98,102]. Additionally, studies showing similarly improved performance for LiF doped organic layers [83,99,103] or thick alternating stacks of LiF and organic films [104] suggest that the mechanism is complicated and multiple factors influence the interfacial energy level alignment.

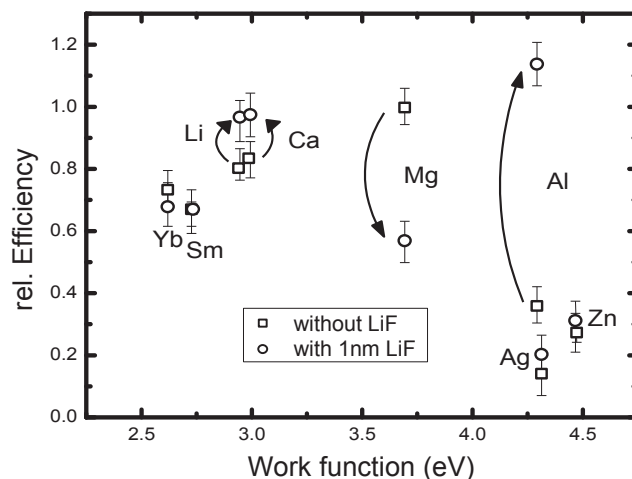


**Figure 3.** Effect of interlayer with a variety of cathodes for relative efficiency for a LiF interlayer. Adapted from Ref. [83] copyright (2000) with permission from Elsevier.

As LiF is a wide band gap insulator [105], it is typically only effective as an interlayer below a critical thickness as an ultrathin layer [19,30,88,95,106–109]. For Al top electrodes, this is generally between 0.5 and 1.5 nm. Above a critical thickness, LiF's capacity to improve charge transfer diminishes, which deteriorates device performance. However, in some cases, the use of thicker LiF layers have shown improved performance, such as 3–5 nm for Ag [110], up to 10 nm with C<sub>60</sub> [91], or between 2 and 50 nm for poly(spirofluorene) [111].

Due to the high surface roughness of typical  $\pi$  conjugated molecular films used in devices, separating the LiF morphology and structure from that of the underlying organic layers can be challenging. Studies have either used indirect methods [112,113] or described island growth on rough surfaces, which obscures and limits information on the coverage and size of the LiF islands [114–116]. However, Turak and co-workers [61,62,117] showed directly by using well ordered small molecules that form large smooth terraces (diindneoperylene, DIP) that, at thicknesses used in typical systems, LiF forms disconnected nanoparticles roughly 0.5 nm in diameter on organic surfaces without disrupting the crystalline packing of the underlying organic layer (see Figure 4). They have observed that LiF deposits as similar sized nanoparticles that coalesce on the surface until a full layer is formed, as on other surfaces. Therefore, for QCM measured thicknesses below 30 Å, the nominal film thickness is less useful than direct observation of the size, distribution and coverage of crystallites when trying to determine the mechanism for LiF as an interlayer.

Though island growth suggests the formation of a complete layer on the surface after approximately 20–30 Å deposition [61,62], the maximum possible useable thickness of the LiF layer in a device is highly dependent on the nature of the underlying organic layer. In most cases, performance is maximized for submonolayer films, but some systems can perform well with extremely thick LiF layers [89,91,103,111,118], as seen in Figure 4c, comparing a device with an Alq<sub>3</sub> ETL to one with a C<sub>60</sub> layer.

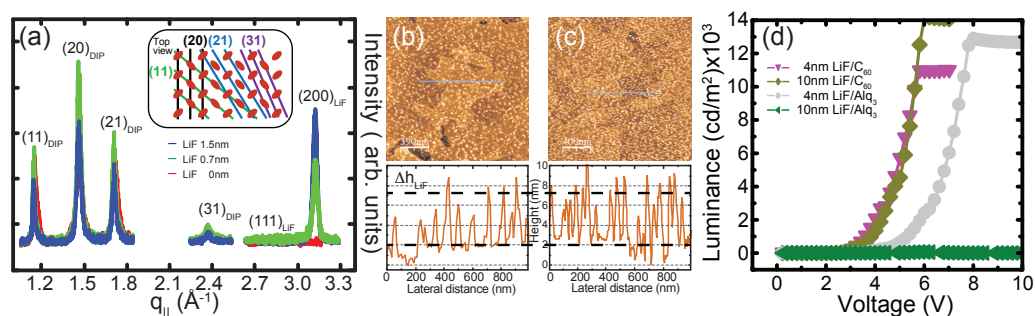


**Figure 4.** Thickness dependent LiF deposition on top of planar monolayer (ML) by monolayer grown di-indenoperylene (DIP) (a) GIXRD data support the formation of crystalline nanoparticles on well ordered organic molecules without disrupting the crystalline packing. Centre positions of the observed in-plane peaks were fitted with Lorentzian functions. Inset shows the schematic arrangement in the observable crystallographic planes in real space for DIP herring bone structure and LiF FCC structure. (b) AFM micrographs of low coverage ( $\sim 7$  Å) and (c) high coverage ( $\sim 15$  Å) show the LiF islands formed on top of the large flat plateau islands of DIP. Height profile beneath corresponds to the line in the AFM micrograph, showing height steps between different DIP layers and peaked height fluctuations ( $20$ – $70$  Å) due to LiF. Reproduced with permission from Ref. [62]. (d) Luminance–voltage (L–V) characteristics of multilayer OLED device with Alq<sub>3</sub> and NBB (C<sub>60</sub>) electron transporting layers with relatively thick LiF layers, which form a complete layer on top of the organic molecule. Though 10 nm completely blocks emission from Alq<sub>3</sub> based devices, the emission characteristics are unchanged for the NBB layer. Device structure glass/ITO/NPB(60 nm)/Alq(25 nm)/NBB(0 or 20 nm)/LiF (4 or 10 nm)/Al(150 nm). Reproduced with permission from Ref. [91].

#### Role of LiF in Top Contact Stability

In addition to its role in improving device performance, LiF interlayers have also been very effective in improving device stability, and its role has been widely studied [8,10,12,34,91,104,119–127]. In general, at the top contact side, buffer layers should block oxygen and moisture, prevent metal diffusion, enhance adhesion, and inhibit interfacial reactions [34]. The best reported improvements in lifetime for LiF interlayers, relative to the electrode without LiF, are given in Table 1. Lifetime, as described previously, is defined as the time for the initial electrical behaviour, either current density or efficiency, to decay to some percentage of its initial value, typically 50% for OLEDs and 80% for OPVs [12,34].

For Al electrodes, LiF improves both lifetime and electrical performance for both OLEDs and OPVs. Turak et al. [8] using X-ray photoelectron spectroscopy (XPS) and Paci et al. [128] with X-ray reflectivity (XRR) showed that sub-monolayers of LiF slow down oxidation at Al surfaces (see Figure 5). Lattante et al. [123] found that LiF stabilized the series resistance in OPVs with exposure to air. Ganzorig et al. [120] saw that dark spot formation rates decrease when bilayer electrodes with LiF are used. Huang et al., and developed further by Turak [34,86], showed that 0.5 nm LiF is sufficient to increase the  $t_{80}$  from 10 to 60 min for single layer diodes, with thicker layers providing better protection [34]. A C<sub>60</sub>/LiF multilayer stack [104], and LiF doping into C<sub>60</sub> [118] and Alq<sub>3</sub> [129] layers for bulk heterojunction devices also improved the device stability, with higher roughness and decreased interfacial injection barriers. However, this improvement is not universal; the accumulation of charged defects within the layer has been suggested to play a role in the catastrophic failure of OLEDs [127], and some metal cathodes, such as Mg and Cu, rapidly degrade when used with a LiF interlayer [8,10,83,91,130].

**Table 1.** Best improvement in the device lifetime,  $t_{50}$  (for OLEDs) and  $t_{80}$  (for OPVs) for LiF used at the top electrode relative to without its use, either as an interlay or an encapsulant.

Interlayer	$t_{50}/t_{80}$	Electrode	ETL	
OLEDs				
LiF	16×	Al	Alq <sub>3</sub>	[120]
LiF	2×	Al	MEH-PPV	[131]
Alq <sub>3</sub> :NPB+LiF	1.3×	Al/LiF	Alq <sub>3</sub> :NPB	[129]
OPVs				
LiF/Cu	1.5×	Cu	C <sub>60</sub>	[130]
LiF/Al	1.2×	Al	MDMO-PPV:PCBM	[128]
CuO/LiF/Al	150×	Al	P3HT:PCBM	[125]
LiF/Al	2.7× ( $t_{90}$ )	Al	P3HT:PCBM	[104]
C <sub>60</sub> :LiF composite/Al	6.2×	Al	P3HT:PCBM	[118]
C <sub>60</sub> /LiF/Al	>3.3× ( $t_{90}$ )	Al	P3HT:PCBM	[104]
encapsulants				
UV+LiF encapsulant	15–25×	Al/LiF	Alq <sub>3</sub>	[132]
LiF (120 nm) encapsulant	11×	Al/LiF	Alq <sub>3</sub>	[132]

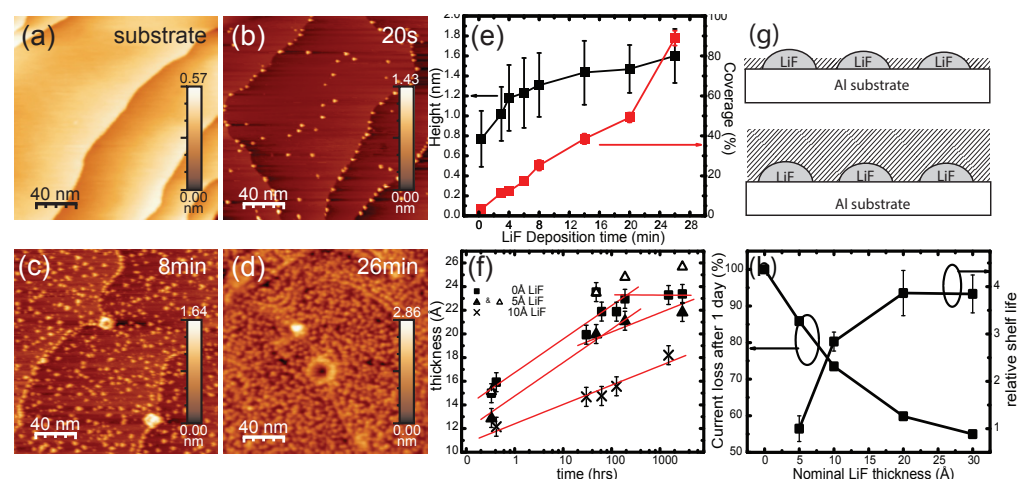


**Figure 5.** AFM micrographs of evaporated LiF films (a) bare Al (100) single crystal (b) after 20 s deposition of LiF (c) after 8 min (d) after 26 min (e) surface coverage and height as a function of LiF deposition time. Reproduced with permission from Springer Nature from Ref. [61] Copyright (2021). (f) Growth of oxide on Al surfaces, monitored by XPS, for thickness as estimated by the simple overlayer model. Lines represent a linear sum of reduced squares best fit of the data for the bare Al surface and the surface with 10 Å LiF deposition. Uncoated Al and 5 Å LiF coated Al both show a bend in the curve at around 60 h. The open triangles represent the predicted oxide values scaled by the LiF coverage as predicted by angle resolved XPS. Reproduced with permission from Ref. [8]. Copyright 2007, The Electrochemical Society. (g) Schematic oxide growth model on LiF coated Al surfaces. (Top) Initially, growth occurs between LiF islands, producing a columnar structure. As growth progresses, Al diffuses through the LiF islands and growth occurs over the islands, leading to (bottom) an embedded structure. (h) The loss of performance after one day, and the shelf life ( $t_{10}$ ) relative to the 0.5 nm LiF interlayer, as a function of LiF thickness for C<sub>60</sub> based OLED devices with Al/xLiF cathodes. The lines are a guide to the eye. Reproduced from Ref. [34] with permission of The Royal Society of Chemistry.

While the impact of LiF is well documented, the mechanisms for stability improvement, such as those for electrical enhancement, are still not completely understood. The effectiveness of LiF in stabilizing the interface also challenges the commonly held belief that dissociation and doping with Li<sup>+</sup> is a dominant mechanism, as such radicals have been proven to be detrimental to device stability [12,34], and would not be expected to

effectively block oxidation of the electrode. Therefore, there does not seem to be a clear mechanism for stability improvement if the LiF layer was dissociated. On the other hand, if LiF was intact, a potential explanation for these disparate effects for different electrodes could be related to interfacial oxidation, as studied by Turak and coworkers [8,10,34,86,91].

In particular, C<sub>60</sub> based diodes with LiF bilayer electrodes using Al and Mg have been helpful to understand the role of LiF [10,34,86,91]. Due to the rapid doping and oxidation of C<sub>60</sub> with exposure to oxygen, such devices decay quickly if unencapsulated. By incorporating a 0.5 nm LiF layer with Al, Huang et al. was able to increase  $t_{80}$  of such devices from 10 to 60 min [86]. However, ultrathin layers of LiF consist of an agglomeration of LiF nanoparticles [61,62] that do not completely cover the surface, as shown in Figure 5. Such a nanoporous LiF layer is not able to prevent electrode oxidation (see Figure 5f) [8], and the device has only 85% of its initial current after exposure to air for 1 day [34]. Increasing the thickness of LiF can limit this current decay, as shown in Figure 5h, which shows the initial current decay and relative unencapsulated shelflife ( $t_{10}$ ) as a function of LiF thickness [34]. In such devices, the current degradation follows a typical decay curve, described by two exponentials [12]. The monotonic decay rate, which sets in after one day exposure to ambient atmosphere, is the same for all thicknesses of LiF [34]. As such, it is likely related to the oxidative degradation of the C<sub>60</sub> layer [133–135]. This oxidation is reversible, as Huang et al. [86] showed that annealing for 24 h in vacuum completely recovers the tunnel diode characteristics for C<sub>60</sub> diodes with a 0.5 nm LiF interlayer with Al electrodes.

The initial decay, on the other hand, is most likely related to the oxidation of the interface. As Turak [34] showed, the initial current loss after one day can be reduced by half by increasing the thickness of LiF to 3 nm (Figure 5h). Chin et al. [119] also observed a thickness dependence in the initial loss of luminance during degradation for OLEDs with LiF/Ca cathodes. The shelf lifetime ( $t_{10}$ ) for C<sub>60</sub> diodes described by Turak [34], heavily affected by that initial current loss, increases with LiF thickness, mirroring the protection provided by the LiF layer against electrode oxidation. For Al electrodes, a 0.5 nm LiF layer does not sufficiently passivate the surface against oxidation (see Figure 5f) [8] due to incomplete coverage, and with similar interlayer thickness, the device still degrades relatively rapidly. Increasing the thickness to 1 nm improves the shelf lifetime by nearly a factor of three [34], which reflects the passivation of the Al surface with 1 nm of LiF observed by Turak et al. [8]. Above 2 nm, which corresponds to the onset of nearly complete coverage as shown by Lee et al. [61], the shelf lifetime becomes independent of the LiF thickness. The fact that oxidation is the dominant decay mechanism is supported by the work of the Krebs group for C<sub>60</sub> based solar cells, where LiF had no impact on the device degradation, when devices were encapsulated [122].

Beyond blocking interfacial oxidation, the LiF layer has also been shown to prevent oxygen and water diffusion into various organic layers, as demonstrated in Grozea et al. and Turak [9,34]. Though Grozea et al. [9] showed that 20 nm of LiF are sufficient to completely block oxygen penetration to the organic layer, Turak [34] saw chemisorbed O and Al throughout the interlayer thickness for thinner layers (Figure 6). With a nanoporous layer consisting of agglomerated nanoparticles on the organic surface [61,62], thinner LiF layers do not completely prevent Al from penetrating into the organic layers, trapping laterally diffusing oxygen atoms away from the injection zone. As a bonus, this effect consumes some of the molecular oxygen that would otherwise act as bulk conduction traps within the C<sub>60</sub> layer itself [135]. Therefore, the LiF interlayer protects the device by both scavenging oxygen within the LiF layer and preventing oxidation at the critical injection region. Gao et al. [118] used this effect to achieve a  $t_{50}$  of 2300 h with a C<sub>60</sub>:LiF composite buffer layer for P3HT:PCBM OPVs.

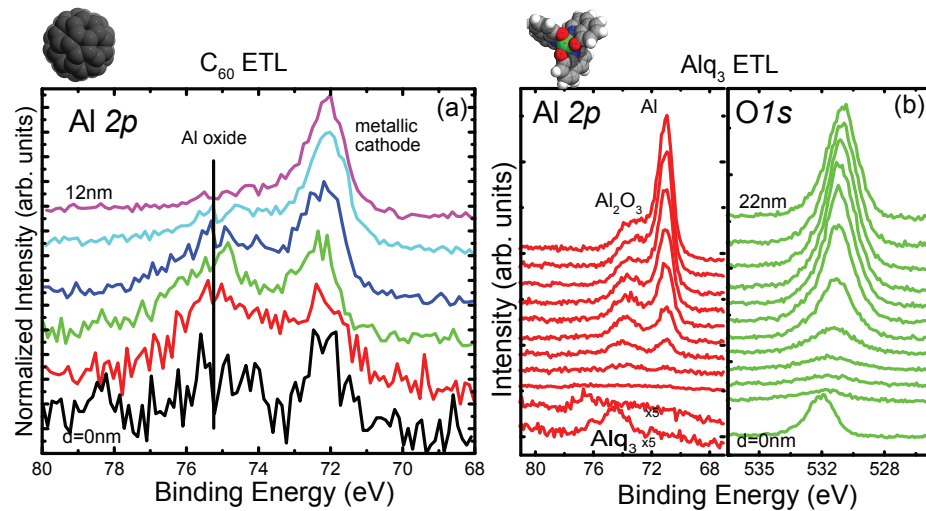


**Figure 6.** (a) XPS Al  $2p$  core level for the sputter profile through the thickness of the LiF layer for peeled Al/10 nm LiF cathodes on  $C_{60}$  based OLEDs, showing the evolution of the chemisorbed Al. Reproduced from Ref. [34] with permission of The Royal Society of Chemistry. (b) XPS depth profile on the Al/LiF side of peeled off interface with 20 nm LiF layer. The evolution of the Al  $2p$ , and O  $1s$  core level features is shown as a function of the distance from the interface. The presence of an Al oxide at the Al/LiF interface suggests diffusion of O through pinholes in the Al films. Such O diffusion ends abruptly at the Al/LiF interface. Adapted from Ref. [9] with the permission of AIP Publishing.

Changing the electrode material, however, can result in completely different behaviours in LiF interlayers. Under mild electrical stress ( $\sim 6$  V), Turak et al. [10] saw significant bubbling and device failure for Mg/LiF electrodes in  $C_{60}$  and  $Alq_3$  based devices. This was thought to be as a result of high Joule heating, from the high barrier to charge injection [34]. Using an in-house developed Scotch tape peel method [91], Turak et al. [10] examined the buried interface, seeing enhanced molecular breakdown of  $Alq_3$  with LiF, corresponding with the observation that LiF on Mg surfaces form bulky carbonates that enhance electrode oxidation [8]. Ghorashi et al. [130] saw that Cu electrodes for  $C_{60}$  based OPVs similarly had worse stability with a LiF interlayer, though they were able to increase the lifetime if the bilayer was exposed to an ambient atmosphere to allow the formation of copper oxides. Therefore, the oxidation behaviour of the interface seems to dictate the effect of LiF for different metal electrodes.

One possible explanation for the disparate performance of different metal/LiF combinations may be attributed to the coherence of the interfacial layers with the metal electrode, using the bulk lattice constants as a rough guide in predicting the oxidation resistance and interface integrity. If an overlayer is not well matched with the underlayer, it may not be able to form a protective barrier at the interface. The distortion in the interface coherence can allow fast diffusion pathways for oxygen and water, increasing the oxidation. The surface lattice constant, assuming  $(1 \times 1)$  surface structure, therefore, could be used to predict which of these interfaces will provide a better contact. In this case, the lattice matching can be defined from a coincidence-site lattice concept [136], where the long and short axes of the surface unit cell for a given plane are matched to gauge the coherence of the interface. The misfit is defined by

$$\Delta = \frac{a_A - a_B}{a_A} \quad (2)$$

where  $a_n$  is the surface lattice constant along a given direction on the surface plane. If the lattices match over a broad range of orientations, the likelihood of the grains having similar, well matched orientations is high. Table 2 shows the lattice mismatch comparisons for low indexed planes for Al/LiF and Mg/LiF bilayers.

At thicknesses typically used in optoelectronic device cathodes, 5–10 Å, evaporated LiF does not completely cover the surface, instead forming islands, as seen in Figure 5 for LiF on single crystal Al. For Al, even without complete surface coverage, LiF is effective in decreasing the oxidation rate due to broadly matched lattices of the overlayer and the substrate, as shown in Table 2. As LiF and Al have good lattice matching over a broad range of orientations, it is likely that, upon deposition, any one of the preferred planes is aligned. The commensurate LiF islands, therefore, give the Al surface a corrugated structure upon which the oxide grows, as in Figure 5, with the islands acting as diffusion barriers for Al atoms. Turak et al. [8] found that ion diffusion was two orders of magnitude faster in the oxide alone compared to the combination of LiF and oxide on the metal surface.

**Table 2.** Lattice constant comparisons for low index planes.

	Lattice Misfit <sup>a</sup>	Best Matched Interface
Al/LiF	0.7%	{100} // {100}, {110} // {110}, {111} // {111}
Mg/LiF	11.3%	{0001} // {111} <sup>b</sup>
Mg/Mg(OH) <sub>2</sub>	1.9%	{0001} // {0001}
	1.9%, 5%	(1 $\bar{1}$ 02) / (1 $\bar{1}$ 02)
Mg/MgCO <sub>3</sub>	30.8%	{0001} // {0001}

<sup>a</sup> Lattice constants  $a_{\text{Al}} = 4.04 \text{ \AA}$  [137],  $a_{\text{LiF}} = 4.02 \text{ \AA}$  [138],  $\frac{a}{c}_{\text{Mg}} = \frac{3.2 \text{ \AA}}{5.2 \text{ \AA}}$  [137],  $\frac{a}{c}_{\text{Mg(OH)}_2} = \frac{3.12 \text{ \AA}}{4.73 \text{ \AA}}$  [139],  $\frac{a}{c}_{\text{MgCO}_3} = \frac{4.632 \text{ \AA}}{15.007 \text{ \AA}}$  [140]. <sup>b</sup> {1000} symmetrically equivalent to {111} [141].

When the Al is deposited on top of the LiF on an organic, such as in device structures, the interfacial chemical structure that develops is related to the amount of protection the LiF can provide for the Al overlayer. As the thickness of LiF increases, the protection of the cathode from oxidation is improved [9]. In a device with 0.5–1.5 nm LiF, the LiF layer is mixed with an oxidized Al layer [34]. When the metal capping layer and the interlayer have good lattice matching, the LiF layer prevents migration of oxygen and acts as a trap for oxygen away from the metal surface.

Deposition of LiF on Mg surfaces, which has poor nearest neighbour lattice matching, has the opposite effect. Rather than passivating the surface, LiF on the surface changes the products of oxidation [8]. Initially, there is preferential oxidation to form MgCO<sub>3</sub> on the surface, with little apparent change in the oxide thickness. As oxidation continues, oxygen and water likely diffuse through the incommensurate LiF lattice, and hydroxides become the dominant oxide components [8]. When this occurs, the oxidation rate increases rapidly, and the oxide thicknesses for the coated and uncoated surfaces become similar. Irrespective of the oxide thickness, the LiF coated surfaces show preferential formation of MgCO<sub>3</sub>. Such carbonates are very poorly lattice matched with Mg. The presence of LiF, therefore, modifies the activity of the metal surface, decreasing the likelihood of Mg(OH)<sub>2</sub> formation.

For Mg devices, which already show a tendency to react with the O rich groups in organometallics [37], the introduction of an LiF interlayer does not protect the Mg from destructive molecular fragmentation reactions, and in fact enhances them, changing the by-products of reaction between Mg and the organic layer [10]. Additionally, oxidation is not prevented at the metal surface, as LiF and Mg are not coherent. Without LiF, the possibility of initially forming Mg(OH)<sub>2</sub> is much higher. Since Mg(OH)<sub>2</sub> has better matching along many orientations, it could help to explain why Mg cathodes perform much better than Mg/LiF cathodes. With bulky, mismatched interfacial reaction products when LiF is present, the injection of electrons appears to be limited and cathode delamination is likely, which results in the complete suppression of luminescence in devices with bilayer cathodes [10,83]. Subsequently, a device incorporating LiF fails almost immediately compared to devices with Mg alone.

The introduction of LiF is not universally beneficial for long term device stability, as the case of Mg/LiF shows. One of the failure mechanisms with Mg/LiF was the delami-

nation of the top electrode, which is another general route for device degradation [12]. In delamination, interfacial defects, interfacial oxidation products or swelling/dissolution of interfacial structures all weaken the adhesion of the top electrode [12]. Defects are particularly troublesome, as in almost all cases, they act as a local avenue for the penetration of moisture and ambient air into the device.

As LiF is hygroscopic [52,142], the agglomerated nanoparticle LiF thin films can be vulnerable to moisture attack and potential dissolution. Turak et al. showed that LiF interlayers significantly decreased the interfacial adhesion for P3HT:PCBM solar cells [11,12], as shown in Figure 7. A Scotch tape peel test for Al on P3HT:PCBM was significantly easier for 20 nm thick LiF interlayers compared to the typical submonolayer films, where immersion in a water bath for at least 10 min was required for complete electrode removal. Without a LiF interlayer, even immersion in a water bath only results in incomplete cathode removal during the peel test, due to the strong adhesion between Al and P3HT:PCBM [11]. Phatak et al. [43] also saw that in high humidity environments, incorporating LiF resulted in faster growth of dark spots. Replacing LiF with insoluble interlayers has been shown to be effective at preventing interfacial delamination [12,43].

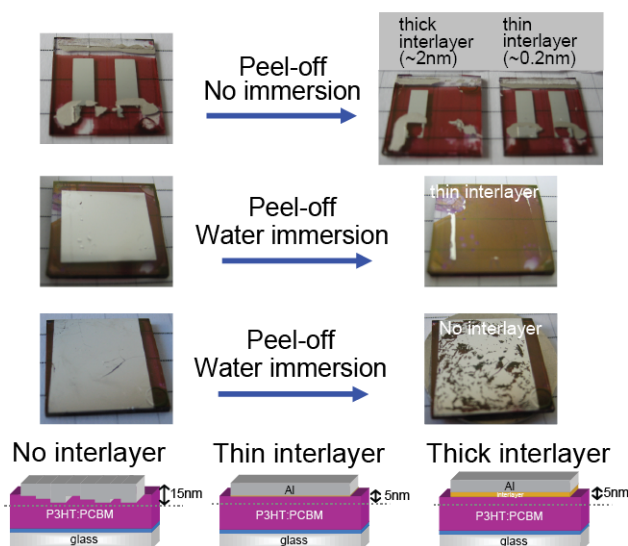


**Figure 7.** Effect of interlayer thickness on interfacial interaction zone and peeling. Optical micrographs of complete devices before (left) and after (right) Scotch tape peeling for various interlayers. At the bottom are schematic models of the interfacial interaction zone and nature of the electrode interface. Reprinted from Ref. [12], copyright (2019) with permission from Elsevier.

### 5. LiF Interlayers at Substrate Contact Interface

Though LiF is more commonly used as an interlayer at the top contact, a number of studies have also shown that LiF can be beneficial at the bottom contact as well. Similar to the top contact, an optimal thicknesses of LiF ranging from 0.5 to 1 nm on ITO has been shown to improve device performance in single carrier devices, OLEDs and OPVs for a variety of hole injection layers, as shown in Figure 8, and outlined in Table 3. LiF nanoparticles decrease the built-in voltage of hole-only devices, resulting in significantly more current at lower bias. Ultrathin layers also affect the peak capacitance voltage, corresponding to the highest density of space charges formed in the device [61,143]. As can be seen from Figure 8b, a more rapid increase in capacitance and a higher peak capacitance at lower voltages is seen with inclusion of a LiF interlayer compared to bare ITO. The steeper increase in capacitance with LiF suggests that the recombination rate is much slower than the carrier injection rate, allowing high density accumulation of injected carriers. This can be used advantageously in both OPVs and OLEDs, where submonolayer coverage of LiF with nanoparticles was shown to significantly increase the short circuit current in

P3HT:PCBM solar cells and improve the luminance from blue phosphorescent OLEDs (Figure 8c,d).

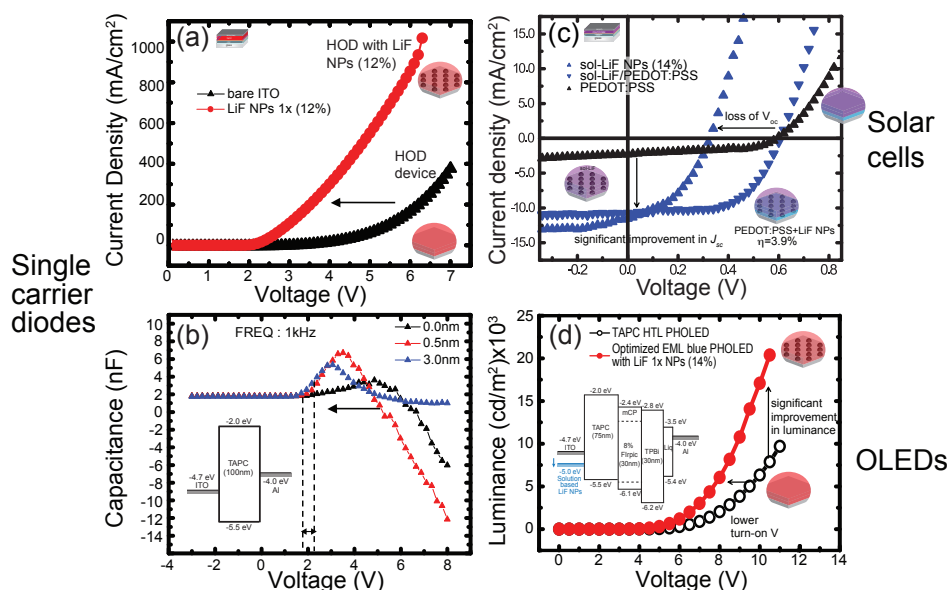


**Figure 8.** (a) Current density–voltage of single layer hole-only devices (HODs) using a TAPC hole transporting layer sandwiched between Al and ITO, with and without solution deposited LiF nanoparticles on the ITO surface. Insets show schematically the device structure and ordered uniform array of nanoparticles. Adapted with permission from Springer Nature from Ref. [61] Copyright (2021). (b) Capacitance–voltage characteristics of single layer hole-only devices (HOD) with submonolayer (0.5 nm) and evaporated LiF and on the ITO electrode. Inset shows the expected energy levels for the device structure. Adapted with permission from Springer Nature from Ref. [61] Copyright (2021). (c) Typical illuminated current density–voltage ( $J$ – $V$ ) curves for polymer–fullerene photovoltaic cells with various anodes. Insets show schematically the device structure and ordered uniform array of nanoparticles. Adapted from Ref. [74] with the permission of AIP Publishing. (d) Luminance–voltage characteristics of blue phosphorescent OLED using a TAPC hole transport layer. Inset shows the expected energy levels for the device structure, as well as the ordered uniform array of nanoparticles. Adapted with permission from Springer Nature from Ref. [61] Copyright (2021).

Improved device performance for LiF at the ITO surface has been attributed to both enhanced and inhibited hole injection, as summarized in Table 3. As a result of its large band gap, LiF is thought to act as a tunnelling layer or a surface blocking layer, dependent on thickness for complete layers. Blocking hole injection can aid in increasing luminance in OLEDs by improving the charge carrier balance [144–146] as generally, electrons have lower mobility than holes in many organic devices. Blocking of exciton dissociation at the electrode surface with LiF has also been proposed, as doing so would prevent leakage currents, leading to enhanced performance [147–149]. The effect of LiF as a tunnelling layer is described by the metal insulator semiconductor model, where charge carriers can tunnel through thin layers with high barriers under an applied field [150–152]; Bory et al. [89] additionally proposed that, for extremely thick layers, the ionized defects in the LiF layer can provide a pathway for enhanced tunnelling. Alternatively, accumulated surface charge at bilayer contacts can polarize the insulating material, for thin or submonolayer films, changing the electrical field and barrier to hole injection in the device dynamically [61,74,153–155]. With a high dipole moment, LiF can effectively tune the energy level alignment by modifying the interface states [61,153–155].

**Table 3.** Comparison of LiF interlayer effects at ITO surfaces. Reprinted with permission from Springer Nature [61] Copyright (2021).

HTLs	HOMO	Thickness of LiF	Effect of LiF on Hole Injection	Mechanism	Reference
TAPC	5.5 eV	submonolayer	Enhanced	Interfacial dipole	[61]
NPB	$5.3 \pm 0.25$ eV	submonolayer	Inhibited	Interfacial dipole	[61]
NPB	$5.3 \pm 0.25$ eV	0.5~1.5 nm	Enhanced/Inhibited (dependent on initial barrier)	Tunnelling	[150]
NPB	$5.3 \pm 0.25$ eV	1 nm	Inhibited	Charge balance	[145]
TPD	5.5 eV	0.4 nm	Inhibited	Charge balance	[146]
CuPc	5.2 eV	1 nm	Enhanced	Interfacial dipole	[155]
CuPc	5.2 eV	3 nm	Enhanced	Exciton dissociation	[149]
CuPc	5.2 eV	1 nm	Enhanced	Exciton dissociation	[147]
CuPc	5.2 eV	0.5–1.5 nm	Enhanced	Tunnelling	[151]
Pentacene	4.9 eV	0.1 nm	Enhanced	Interfacial dipole	[154]
P3HT:PCBM	5.2 eV	nanoparticles	Enhanced	Interfacial dipole	[74]
P3HT	5.2 eV	5 nm	Enhanced	Ionization of defects	[89]
PEDOT	$5.1 \pm 0.1$ eV	0.5 nm	Inhibited	Charge balance	[144]
PEDOT	$5.1 \pm 0.1$ eV	0.5 1.5 nm	Enhanced	Tunnelling	[152]
PEDOT	$5.1 \pm 0.1$ eV	nanoparticles	Enhanced	Interfacial dipole	[74,153]

Lee et al. [61] recently showed that in hole only devices, submonolayer LiF is necessary for enhanced current density, particularly for large band gap, deep HOMO HTLs with large injection barriers. For incomplete LiF layers, the high dipole moment and polarization enhances the hole injection [6,7,61]; once the coverage is complete, tunnelling probability decreases as thickness increases, as observed in other studies [150–152]. By deliberately introducing LiF nanoparticles with controlled submonolayer coverage using reverse micelle templating, Lee et al. [61] showed hole injection much higher than what can be achieved with thermal evaporation of LiF (see Figure 9a). Using this enhanced hole injection in blue PHOLEDs with large band gap hole transport layers, they improved luminance and efficiency by over 20% (Figure 8d). Similarly, Kurt et al. were able to nearly double the short circuit current of polymer-fullerene solar cells, increasing the efficiency by 70% [153] as shown in Figure 9b with a submonolayer of micelle templated LiF.

However, as with LiF at the top interface, this behaviour is not universal. Lee et al. [61] and Zhao et al. [150] showed that the initial barrier to hole injection has a big effect on the utility of LiF. For hole transporting layers with relatively shallow HOMOs, no improvement in light emission was observed (see Figure 9c).

Though work function tuning of the ITO interface has been possible using solution deposited LiF [6,7,153], as shown in Figure 9d, which was taken advantage of by Kurt et al. [153] for P3HT:PCBM solar cells (see Figure 9b), capacitance and single carrier device analysis by Lee et al. [61] suggests that static vacuum work function values determined ex situ do not represent the true barrier to injection in the device, due to the dynamic nature of interface dipoles during device performance. Instead, it seems that quasi-ordered nanoparticles of uniform size at the ITO surface tunes the interface and trap states, modifying the electric field developed in the subsequently deposited organic layers. Resulting from their regular size and spacing, such nanoparticles increase the pathways for injection. The periodic nature of the roughness due to the particles results in an increase in injection and performance [61], rather than the shorting and loss of performance usually attributed to randomly rough surfaces as described in Turak [35].

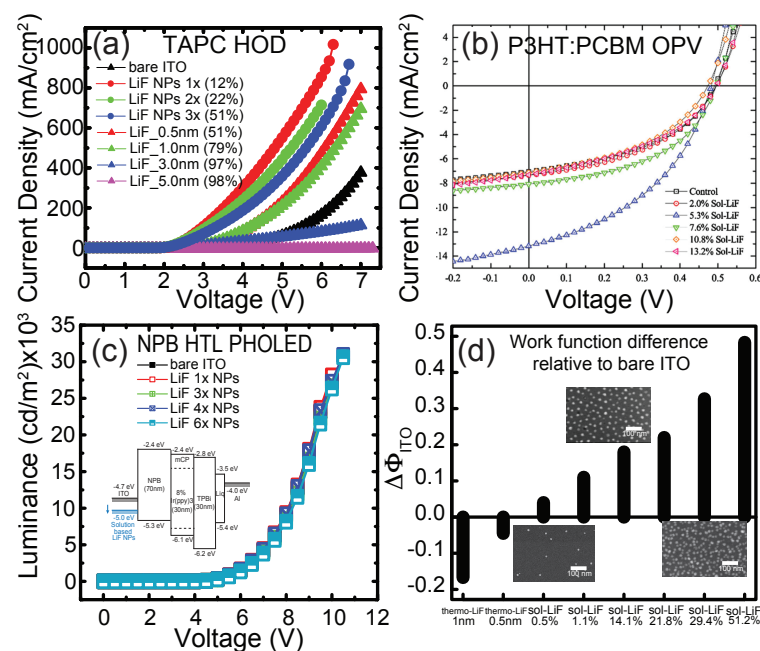


**Figure 9.** (a) Hole only current density–voltage characteristics for various coverages of LiF with a TAPC HOD with a deep HOMO level relative to ITO. Reprinted with permission from Springer Nature from Ref. [61] Copyright (2021). (b) Current density–voltage characteristic curves of P3HT:PCBM solar cells with ITO anodes modified by different sol-LiF surface coverages, a under AM1.5G illumination. Reprinted with permission from Springer Nature from Ref. [153] Copyright (2015). (c) Luminance–voltage characteristics for blue PHOLED devices with an NPB hole transport layer with varying amounts of solution deposited LiF nanoparticles.  $Nx$  represents the number of spin-coating and plasma etching cycles were performed. Reprinted with permission from Springer Nature from Ref. [61] Copyright (2021). (d) Work function difference for various LiF coverages relative to bare ITO. Insets show SEM images of representative LiF decorated surfaces. Note that measurements suggest that thermally evaporated LiF decreases the work function of ITO as discussed in [7], which should lead to an increasing barrier to hole injection and solution deposited LiF increases it as a function of coverage (also discussed in [6]), leading to a decreasing barrier.

As with deposition of LiF on top of organic films, the nominal film thickness is less useful than direct observation of the size and distribution of crystallites when trying to determine the mechanism for LiF on the surface. As evaporation conditions can affect the crystallite size [61,62], and every evaporation system is unique, reported QCM thickness values are inadequate to fully correlate with the device behaviour. Using reverse micelle templating, Lee et al. [61] established a categorization of the behaviour of the LiF layer at ITO into different regimes dependent on the surface coverage. At low coverage of nanoparticles, the barrier is low and injection of holes is maximized, and decreases with increasing coverage of LiF. Above a critical surface coverage ( $\sim 50\%$ ), the particles start to act more like a tunnelling layer, with the barrier to injection becoming higher than that at a bare ITO surface, but is mediated by interfacial trap states. Interfacial dipoles in the array of particles induce intermediate states that allow carriers to hop to the bulk states, even after nearly complete coverage is obtained. Further growth of LiF starts to build up multiple porous nanoparticle layers on the surface. Eventually, the layer becomes so thick and the barrier so high that charge carriers cannot be effectively injected and the device does not operate.

#### Role of LiF in Stabilizing Degradation at Bottom Contact Surfaces

Similarly to the introduction of LiF at the top contact, the bottom contact interlayers of LiF often have a secondary effect of modifying the degradation properties. Lee et al. [151], for example, saw a  $1.6\times$  ( $t_{80}$ ) improvement in the lifetime of flexible Alq<sub>3</sub> OLEDs with a

CuPc hole transport layer by introducing thin LiF interlayers. Typically, bottom contact buffer layers can eliminate problems from mechanical weakness and block oxidation or indium diffusion [12,34]. Though there have been few studies on mechanisms for a LiF interlayer specifically, it is likely that these effects would be observed with a LiF interlayer, similar to that observed at the top contact.

One of the main sources of device degradation at the bottom contact and the hole transport layers is morphological instability, with crystallization and dewetting leading to loss of device performance [12,34,35]. Doping with LiF nanoparticles [156,157] been used to prevent dewetting and crystallization in hole transport layers, though enhanced stability sometimes led to decreased device performance for such systems [156]. As stabilization is linked to the strong electrostatic or charge-transfer interactions between the particle and the organic layer leading to a cross-linked network [156,158], the uniform suspension of nanoparticles in the layer can sometimes also disrupt the percolation path of the charge carriers. Yet, doping was not seen to improve stability with every organic, irrespective of the effect on the electrical behaviour. Grozea et al. [156] observed that LiF doping suppressed crystallization of NPB at 120 °C (see Figure 10), while having no impact on the crystallization behaviour of CuPc. Immobilized fillers are thought to be the most effective in stabilizing films, either being pinned to the substrate [158,159], or at grain boundaries [157]. Heidkamp et al. [157] was able to stabilize the dewetting behaviour of DIP by depositing LiF on-top, using the pinning effects of nanoparticles at organic grain boundaries, as shown in Figure 10. Other stabilization mechanisms proposed include the high volume–surface area ratio of the nanoparticles modifying the film rheology and increasing the glass transition temperatures, nanoparticles blocking heterogeneous nucleation of the organic film, and de-segregation of filler and film relieving residual stress [160].

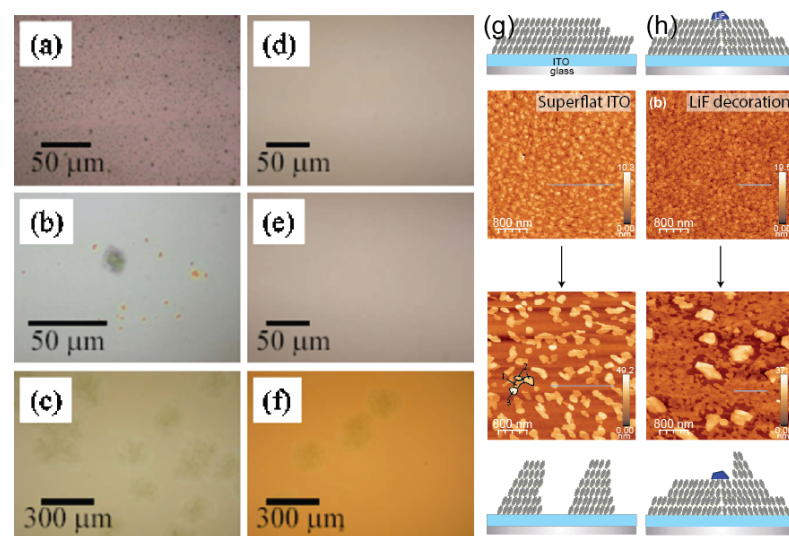


**Figure 10.** Optical micrographs of (a–c) an undoped ITO/NPB 10 nm/NPB 50 nm sample morphology: (a) before annealing, (b) after 120 °C annealing, and (c) after 140 °C annealing; and (d–f) of an ITO/NPB:LiF (5 wt %) 10 nm/NPB 50 nm sample morphology: (d) before annealing, (e) after 120 °C annealing, and (f) after 140 °C annealing. Reprinted from Ref. [156], with the permission of AIP Publishing. (g) Morphology of neat di-indenoperylene (DIP) deposited on superflat ITO. (h) Morphology of DIP on superflat ITO with thermally evaporated LiF nanoparticle decoration. Top panels are the as-deposited morphology, middle panels are AFM micrographs before and after at least one month storage in an evacuated dessicator. The bottom panels show the schematic of DIP structure with significant dewetting of DIP on ITO, stabilized by LiF nanoparticle pinning at DIP grain boundaries. Lines indicate height profiles (not shown). Adapted from Ref. [157], copyright (2013) with permission from SPIE.

## 6. Conclusions

LiF is nearly ubiquitous in all organic optoelectronic devices. Though many materials have been investigated, it has been hard to replace LiF as a dominant interlayer material, as it is relatively stable and easy to evaporate and also deposit from solution in the form of nanoparticles and thin films. Its interesting impacts and sometimes unexpected effects on performance and stability of organic devices has prompted much study and opened up new avenues of research. The role that LiF plays in organic devices is a central one, and with the introduction of organic layers in other exotic devices, including perovskite and quantum dot electronics, it is likely to be an area of continued research for years to come.

**Funding:** This research was funded by a Canada Graduate Scholarship (NSERC), DAAD Research grant (A/05/14232), Marie Curie International Incoming Fellowship within the 7th European Community Framework Programme (LiFOrgPV 221165), European Reintegration Grant within the 7th European Community Framework Programme (NIOS 276963), NSERC Discovery grant (436100-2013 RGPIN), and Early Researcher Award (ER15-11-123, Ontario Ministry of Research and Innovation).

**Institutional Review Board Statement:** Not applicable.

**Informed Consent Statement:** Not applicable.

**Data Availability Statement:** The data presented in this study are available on request from the corresponding author.

**Acknowledgments:** The authors would like to acknowledge the work of various collaborators and students at the Department of Materials Science and Engineering, University of Toronto, Department of Low Dimensional and Metastable Materials, Max-Planck-Institute for Metals Research, Faculty of Engineering and Natural Science, Sabanci University, and the Department of Engineering Physics, McMaster University for access to published and unpublished data.

**Conflicts of Interest:** The authors declare no conflict of interest.

## References

1. Tremblay, J.F. The Rise of OLED Displays. *Chem. Eng. News* **2016**, *94*, 30–34.
2. Liu, Q.; Jiang, Y.; Jin, K.; Qin, J.; Xu, J.; Li, W.; Xiong, J.; Liu, J.; Xiao, Z.; Sun, K.; et al. 18% Efficiency Organic Solar Cells. *Sci. Bull.* **2020**, *65*, 272–275. [CrossRef]
3. NREL. Best Research Cell Efficiencies. 2020. Available online: <https://www.nrel.gov/pv/cell-efficiency.html> (accessed on 17 April 2021).
4. Shaheen, S.E.; Jabbour, G.E.; Morrell, M.M.; Kawabe, Y.; Kippelen, B.; Peyghambarian, N.; Nabor, M.F.; Schlaf, R.; Mash, E.A.; Armstrong, N.R. Bright Blue Organic Light-Emitting Diode with Improved Color Purity Using a LiF/Al Cathode. *J. Appl. Phys.* **1998**, *84*, 2324–2327. [CrossRef]
5. Schlaf, R.; Parkinson, B.A.; Lee, P.A.; Nebesny, K.W.; Jabbour, G.E.; Kippelen, B.; Peyghambarian, N.; Armstrong, N.R. Photoemission Spectroscopy of LiF Coated Al and Pt Electrodes. *J. Appl. Phys.* **1998**, *84*, 6729–6736. [CrossRef]
6. Ow-Yang, C.; Jia, J.; Aytun, T.; Zamboni, M.; Turak, A.; Saritas, K.; Shigesato, Y. Work Function Tuning of Tin-Doped Indium Oxide Electrodes with Solution-Processed Lithium Fluoride. *Thin Solid Films* **2014**, *559*, 58–63. [CrossRef]
7. Aytun, T.; Turak, A.; Baikie, I.; Halek, G.; Ow-Yang, C.W. Solution-Processed LiF for Work Function Tuning in Electrode Bilayers. *Nano Lett.* **2012**, *12*, 39–44. [CrossRef]
8. Turak, A.; Huang, C.J.; Grozea, D.; Lu, Z.H. Oxidation of LiF-Coated Metal Surfaces. *J. Electrochem. Soc.* **2007**, *154*, H691–H697. [CrossRef]
9. Grozea, D.; Turak, A.; Feng, X.D.; Lu, Z.H.; Johnson, D.; Wood, R. Chemical Structure of Al/LiF/Alq Interfaces in Organic Light-Emitting Diodes. *Appl. Phys. Lett.* **2002**, *81*, 3173–3175. [CrossRef]
10. Turak, A.; Grozea, D.; Huang, C.; Lu, Z.H. Interfacial Structure in Organic Optoelectronics. *arXiv* **2005**, arXiv:1208.0321.
11. Turak, A.; Hanisch, J.; Ahlswede, E.; Barrena, E.; Dosch, H. Interfacial Adhesion in Polymer Blend P3HT:PCBM Solar Cells. Fruhjahrstagung DPG. 2009. Available online: <https://www.dpg-verhandlungen.de/year/2009/conference/dresden/part/syop/session/1/contribution/4> (accessed on 31 May 2021).
12. Turak, A. Device Stability in Organic Optoelectronics. In *Handbook of Organic Materials for Electronic and Photonic Devices*, 2nd ed.; Ostroverkhova, O., Ed.; Woodhead Publishing Series in Electronic and Optical Materials; Woodhead Publishing: Cambridge, UK, 2019; pp. 599–662. [CrossRef]
13. Tang, C.W. Two-Layer Organic Photovoltaic Cell. *Appl. Phys. Lett.* **1986**, *48*, 183–185. [CrossRef]
14. Tang, C.W.; van Slyke, S.A. Organic Electroluminescent Diodes. *Appl. Phys. Lett.* **1987**, *51*, 913–915. [CrossRef]

15. Shen, Y.; Klein, M.W.; Jacobs, D.B.; Scott, J.C.; Malliaras, G.G. Mobility-Dependent Charge Injection into an Organic Semiconductor. *Phys. Rev. Lett.* **2001**, *86*, 3867–3870. [[CrossRef](#)]
16. Baldo, M.A.; Forrest, S.R. Interface-Limited Injection in Amorphous Organic Semiconductors. *Phys. Rev. B* **2001**, *64*, 085201. [[CrossRef](#)]
17. Lee, S.T.; Gao, Z.Q.; Hung, L.S. Metal Diffusion from Electrodes in Organic Light-Emitting Diodes. *Appl. Phys. Lett.* **1999**, *75*, 1404–1406. [[CrossRef](#)]
18. Ohno, T.R.; Chen, Y.; Harvey, S.E.; Kroll, G.H.; Weaver, J.H.; Haufler, R.E.; Smalley, R.E. C60 Bonding and Energy-Level Alignment on Metal and Semiconductor Surfaces. *Phys. Rev. B* **1991**, *44*, 13747–13755. [[CrossRef](#)]
19. Hung, L.; Tang, C.W.; Mason, M.G. Enhanced Electron Injection in Organic Electroluminescence Devices Using an Al/LiF Electrode. *Appl. Phys. Lett.* **1997**, *70*, 152. [[CrossRef](#)]
20. Crispin, X.; Geskin, V.; Crispin, A.; Cornil, J.; Lazzaroni, R.; Salaneck, W.R.; Brédas, J.L. Characterization of the Interface Dipole at Organic/Metal Interfaces. *J. Am. Chem. Soc.* **2002**, *124*, 8131–8141. [[CrossRef](#)]
21. Koch, N.; Kahn, A.; Ghijsen, J.; Pireaux, J.J.J.; Schwartz, J.; Johnson, R.L.; Elschner, A. Conjugated Organic Molecules on Metal versus Polymer Electrodes: Demonstration of a Key Energy Level Alignment Mechanism. *Appl. Phys. Lett.* **2003**, *82*, 70–72. [[CrossRef](#)]
22. Kahn, A.; Koch, N.; Gao, W. Electronic Structure and Electrical Properties of Interfaces between Metals and  $\pi$ -Conjugated Molecular Films. *J. Polym. Sci. Part B Polym. Phys.* **2003**, *41*, 2529–2548. [[CrossRef](#)]
23. Braun, S.; Salaneck, W.R.; Fahlman, M. Energy-Level Alignment at Organic/Metal and Organic/Organic Interfaces. *Adv. Mater.* **2009**, *21*, 1450–1472. [[CrossRef](#)]
24. Vázquez, H.; Dappe, Y.J.; Ortega, J.; Flores, F. Energy Level Alignment at Metal/Organic Semiconductor Interfaces: “Pillow” Effect, Induced Density of Interface States, and Charge Neutrality Level. *J. Chem. Phys.* **2007**, *126*, 144703. [[CrossRef](#)] [[PubMed](#)]
25. Vázquez, H.; Flores, F.; Kahn, A. Induced Density of States Model for Weakly-Interacting Organic Semiconductor Interfaces. *Org. Electron.* **2007**, *8*, 241–248. [[CrossRef](#)]
26. Oehzelt, M.; Koch, N.; Heimel, G. Organic Semiconductor Density of States Controls the Energy Level Alignment at Electrode Interfaces. *Nat. Commun.* **2014**, *5*, 4174. [[CrossRef](#)]
27. Kiguchi, M.; Arita, R.; Yoshikawa, G.; Tanida, Y.; Katayama, M.; Saiki, K.; Koma, A.; Aoki, H. Metal-Induced Gap States at Well Defined Alkali-Halide/Metal Interfaces. *Phys. Rev. Lett.* **2003**, *90*, 196803. [[CrossRef](#)]
28. Kiguchi, M.; Yoshikawa, G.; Ikeda, S.; Saiki, K. Electronic Properties of Metal-Induced Gap States Formed at Alkali-Halide/Metal Interfaces. *Phys. Rev. B* **2005**, *71*, 153401. [[CrossRef](#)]
29. Kiguchi, M.; Arita, R.; Yoshikawa, G.; Tanida, Y.; Ikeda, S.; Entani, S.; Nakai, I.; Kondoh, H.; Ohta, T.; Saiki, K.; et al. Metal-Induced Gap States in Epitaxial Organic-Insulator/Metal Interfaces. *Phys. Rev. B* **2005**, *72*. [[CrossRef](#)]
30. Ganzorig, C.; Suga, K.; Fujihira, M. Alkali Metal Acetates as Effective Electron Injection Layers for Organic Electroluminescent Devices. *Mater. Sci. Eng. B* **2001**, *85*, 140–143. [[CrossRef](#)]
31. Heil, H.; Steiger, J.; Karg, S.; Gastel, M.; Ortner, H.; von Seggern, H.; Stößel, M. Mechanisms of Injection Enhancement in Organic Light-Emitting Diodes through an Al/LiF Electrode. *J. Appl. Phys.* **2001**, *89*, 420–424. [[CrossRef](#)]
32. Krebs, F.C.; Norrman, K. Analysis of the Failure Mechanism for a Stable Organic Photovoltaic during 10,000 h of Testing. *Prog. Photovolt.* **2007**, *15*, 697–712. [[CrossRef](#)]
33. Brabec, C.J.; Hauch, J.A.; Schilinsky, P.; Waldauf, C. Production Aspects of Organic Photovoltaics and Their Impact on the Commercialization of Devices. *MRS Bull.* **2005**, *30*, 50–52. [[CrossRef](#)]
34. Turak, A. Interfacial Degradation in Organic Optoelectronics. *RSC Adv.* **2013**, *3*, 6188–6225. [[CrossRef](#)]
35. Turak, A. Dewetting Stability of ITO Surfaces in Organic Optoelectronic Devices. In *Optoelectronics: Advanced Materials and Devices*; Pyshkin, S., Ed.; InTech Open: Rijeka, Croatia, 2013; pp. 229–268.
36. Burrows, P.E.; Bulovic, V.; Forrest, S.R.; Sapochak, L.S.; McCarty, D.M. Reliability and Degradation of Organic Light Emitting Devices. *Appl. Phys. Lett.* **1994**, *65*, 2922–2924. [[CrossRef](#)]
37. Turak, A.; Grozea, D.; Feng, X.D.; Lu, Z.H.; Aziz, H.; Hor, A.M.M. Metal/AlQ(3) Interface Structures. *Appl. Phys. Lett.* **2002**, *81*, 766–768. [[CrossRef](#)]
38. Aziz, H.; Popovic, Z.D.; Tripp, C.P.; Hu, N.X.; Hor, A.M.; Xu, G. Degradation Processes at the Cathode/Organic Interface in Organic Light Emitting Devices with Mg:Ag Cathodes. *Appl. Phys. Lett.* **1998**, *72*, 2642–2644. [[CrossRef](#)]
39. Sato, Y.; Kanai, H. Stability of Organic Electroluminescent Diodes. *Mol. Cryst. Liq. Cryst.* **1994**, *253*, 143–150. [[CrossRef](#)]
40. McElvain, J.; Antoniadis, H.; Hueschen, M.R.; Miller, J.N.; Roitman, D.M.; Sheats, J.R.; Moon, R.L. Formation and Growth of Black Spots in Organic Light-Emitting Diodes. *J. Appl. Phys.* **1996**, *80*, 6002–6007. [[CrossRef](#)]
41. Liew, Y.F.; Aziz, H.; Hu, N.X.; Chan, H.S.O.; Xu, G.; Popovic, Z. Investigation of the Sites of Dark Spots in Organic Light-Emitting Devices. *Appl. Phys. Lett.* **2000**, *77*, 2650–2652. [[CrossRef](#)]
42. Schaer, M.; Nüesch, F.; Berner, D.; Leo, W.; Zuppiroli, L. Water Vapor and Oxygen Degradation Mechanisms in Organic Light Emitting Diodes. *Adv. Funct. Mater.* **2001**, *11*, 116–121. [[CrossRef](#)]
43. Phatak, R.; Tsui, T.Y.; Aziz, H. Dependence of Dark Spot Growth on Cathode/organic Interfacial Adhesion in Organic Light Emitting Devices. *J. Appl. Phys.* **2012**, *111*, 054512. [[CrossRef](#)]

44. Emerson, J.A.; Toolan, D.T.W.; Howse, J.R.; Furst, E.M.; Epps, T.H. Determination of Solvent–Polymer and Polymer–Polymer Flory–Huggins Interaction Parameters for Poly(3-Hexylthiophene) via Solvent Vapor Swelling. *Macromolecules* **2013**, *46*, 6533–6540. [[CrossRef](#)]
45. Vasilak, L.; Tanu Halim, S.M.; Das Gupta, H.; Yang, J.; Kamperman, M.; Turak, A. Statistical Paradigm for Organic Optoelectronic Devices: Normal Force Testing for Adhesion of Organic Photovoltaics and Organic Light-Emitting Diodes. *ACS Appl. Mater. Interfaces* **2017**, *9*, 13347–13356. [[CrossRef](#)] [[PubMed](#)]
46. Velthuizen, J.V.; Chao, G.Y. Griceite, LiF, a New Mineral Species from Mont Saint-Hilaire, Quebec. *Can. Mineral.* **1989**, *27*, 125–127.
47. Thewlis, J. Unit-Cell Dimensions of Lithium Fluoride Made from Li6 and Li7. *Acta Crystallogr.* **1955**, *8*, 36–38. [[CrossRef](#)]
48. Wharton, L.; Klemperer, W.; Gold, L.P.; Strauch, R.; Gallagher, J.J.; Derr, V.E. Microwave Spectrum, Spectroscopic Constants, and Electric Dipole Moment of Li6F19. *J. Chem. Phys.* **1963**, *38*, 1203–1210. [[CrossRef](#)]
49. Klocek, P. *Handbook of Infrared Optical Materials*; Marcel Dekker: New York, NY, USA, 1991.
50. Angel, D.W.; Hunter, W.R.; Tousey, R.; Hass, G. Extreme Ultraviolet Reflectance of LiF-Coated Aluminum Mirrors. *J. Opt. Soc. Am.* **1961**, *51*, 913. [[CrossRef](#)]
51. Cox, J.T.; Hass, G.; Waylonis, J.E. Further Studies on LiF-Overcoated Aluminum Mirrors with Highest Reflectance in the Vacuum Ultraviolet. *Appl. Opt.* **1968**, *7*, 1535. [[CrossRef](#)]
52. Fleming, B.; Quijada, M.; Hennessy, J.; Egan, A.; Hoyo, J.D.; Hicks, B.A.; Wiley, J.; Kruczek, N.; Erickson, N.; France, K. Advanced Environmentally Resistant Lithium Fluoride Mirror Coatings for the next Generation of Broadband Space Observatories. *Appl. Opt.* **2017**, *56*, 9941–9950. [[CrossRef](#)]
53. Wang, Y.M.; Wong, K.W.; Lee, S.T.; Nishitani-Gamo, M.; Sakaguchi, I.; Loh, K.P.; Ando, T. Recent Studies on Diamond Surfaces. *Diam. Relat. Mater.* **2000**, *9*, 1582–1590. [[CrossRef](#)]
54. Nadeau, J.S.; Johnston, W.G. Hardening of Lithium Fluoride Crystals by Irradiation. *J. Appl. Phys.* **1961**, *32*, 2563–2565. [[CrossRef](#)]
55. Montereali, R.M.; Almaviva, S.; Bonfigli, F.; Cricenti, A.; Faenov, A.; Flora, F.; Gaudio, P.; Lai, A.; Martellucci, S.; Nichelatti, E.; et al. Lithium Fluoride Thin-Film Detectors for Soft X-ray Imaging at High Spatial Resolution. *Nucl. Instrum. Methods Phys. Res. Sect. A Accel. Spectrometers Detect. Assoc. Equip.* **2010**, *623*, 758–762. [[CrossRef](#)]
56. Flora, F.; Baldacchini, G.; Bonfigli, F.; Lai, A.; Marolo, T.; Mezi, L.; Montereali, R.M.; Murra, D.; Lisi, N.; Nichelatti, E.; et al. Lithium Fluoride Coloration by Laser-Plasma Soft X-rays: A Promising Tool for X-ray Microscopy and Photonics. In *Laser-Generated and Other Laboratory X-ray and EUV Sources, Optics, and Applications*; International Society for Optics and Photonics: Bellingham, WA, USA, 2004; Volume 5196, pp. 298–310. [[CrossRef](#)]
57. Cosset, F.; Celerier, A.; Barelaud, B.; Vareille, J.C. Thin Reactive LiF Films for Nuclear Sensors. *Thin Solid Films* **1997**, *303*, 191–195. [[CrossRef](#)]
58. Kojima, H. Melting Points of Inorganic Fluorides. *Can. J. Chem.* **1968**, *46*, 2968–2971. [[CrossRef](#)]
59. Schulz, L.G. The Structure and Growth of Evaporation LiF and NaCl Films on Amorphous Substrates. *J. Chem. Phys.* **1949**, *17*, 1153–1162. [[CrossRef](#)]
60. Carpenter, R.; Campbell, D.S. Stress in Alkali Halide Films. *J. Mater. Sci.* **1967**, *2*, 173–183. [[CrossRef](#)]
61. Lee, S.I.; Liang, K.; Hui, L.S.; Arbi, R.; Munir, M.; Lee, S.J.; Kim, J.W.; Kim, K.J.; Kim, W.Y.; Turak, A. Necessity of Submonolayer LiF Anode Interlayers for Improved Device Performance in Blue Phosphorescent OLEDs. *J. Mater. Sci. Mater. Electron.* **2021**, *32*, 1161–1177. [[CrossRef](#)]
62. Maye, F. Morphological and Structural Study of Ultrathin Lithium Fluoride Films on Organic Molecule Surfaces. Ph.D. Thesis, University of Stuttgart, Stuttgart, Germany, 2011.
63. Gótek, F.; Mazur, P. LiF Thin Layers on Si(100) Studied by ESD, LEED, AES, and AFM. *Surf. Sci.* **2003**, *541*, 173–181. [[CrossRef](#)]
64. Montereali, R.M.; Baldacchini, G.; Martelli, S.; Do Carmo, L.S. LiF Films: Production and Characterization. *Thin Solid Films* **1991**, *196*, 75–83. [[CrossRef](#)]
65. Butman, M.F.; Smirnov, A.A.; Kudin, L.S.; Munir, Z.A. Mass-Spectrometric Study of the Temperature Variation in the Dimer-to-Monomer Ratio in the Free-Surface Vaporization Fluxes from Alkali Halide Single Crystals. *J. Mater. Synth. Process.* **2000**, *8*, 93–100. [[CrossRef](#)]
66. Dabringhaus, H.; Meyer, H.J. Investigation of Condensation and Evaporation of Alkali Halide Crystals by Molecular Beam Methods: VIII. Molecular Beam Pulse Experiments with Lithium Fluoride. *J. Cryst. Growth* **1983**, *61*, 85–90. [[CrossRef](#)]
67. Cremona, M.; Mauricio, M.; Scavarda Do Carmo, L.; Prioli, R.; Nunes, V.; Zanette, S.; Caride, A.; Albuquerque, M. Grain Size Distribution Analysis in Polycrystalline LiF Thin Films by Mathematical Morphology Techniques on AFM Images and X-ray Diffraction Data. *J. Microsc.* **2000**, *197*, 260–267. [[CrossRef](#)] [[PubMed](#)]
68. Di Nunzio, P.E.; Fornarini, L.; Martelli, S.; Montereali, R.M. Texture Analysis of LiF Thin Films Evaporated onto Amorphous Substrates at Different Temperatures. *Phys. Status Solidi Appl. Res.* **1997**, *164*, 747–756. [[CrossRef](#)]
69. Yamawaki, M.; Hirai, M.; Yasumoto, M.; Kanno, M. Mass Spectrometric Study of Vaporization of Lithium Fluoride. *J. Nucl. Sci. Technol.* **1982**, *19*, 563–570. [[CrossRef](#)]
70. Rupp, M.; Ahlrichs, R. Theoretical Investigation of Structure and Stability of Oligomers of LiH, NaH, LiF, and NaF. *Theoret. Chim. Acta* **1977**, *46*, 117–127. [[CrossRef](#)]
71. Snelson, A. Heats of Vaporization of the Lithium Fluoride Vapor Species by the Matrix Isolation Technique. *J. Phys. Chem.* **1969**, *73*, 1919–1928. [[CrossRef](#)]

72. Perea, A.; Gonzalo, J.; Afonso, C.N.; Martelli, S.; Montekali, R.M. On the Growth of LiF Films by Pulsed Laser Deposition. *Appl. Surf. Sci.* **1999**, *138–139*, 533–537. [[CrossRef](#)]
73. Henley, S.; Ashfold, M.; Pearce, S. The Structure and Composition of Lithium Fluoride Films Grown by Off-Axis Pulsed Laser Ablation. *Appl. Surf. Sci.* **2003**, *217*, 68–77. [[CrossRef](#)]
74. Turak, A.; Aytun, T.; Ow-Yang, C.W. Solution Processed LiF Anode Modification for Polymer Solar Cells. *Appl. Phys. Lett.* **2012**, *100*, 253303. [[CrossRef](#)]
75. Stöbel, M.; Staudigel, J.; Steuber, F.; Simmerer, J.; Winnacker, A. Impact of the Cathode Metal Work Function on the Performance of Vacuum-Deposited Organic Light Emitting-Devices. *Appl. Phys. A* **1999**, *68*, 387–390. [[CrossRef](#)]
76. Rajagopal, A.; Kahn, A. Photoemission Spectroscopy Investigation of Magnesium–Alq<sub>3</sub> Interfaces. *J. Appl. Phys.* **1998**, *84*, 355–358. [[CrossRef](#)]
77. Gu, G.; Parthasarathy, G.; Burrows, P.E.; Tian, P.; Hill, I.G.; Kahn, A.; Forrest, S.R. Transparent Stacked Organic Light Emitting Devices. I. Design Principles and Transparent Compound Electrodes. *J. Appl. Phys.* **1999**, *86*, 4067–4075. [[CrossRef](#)]
78. Song, W.; So, S.K.; Moulder, J.; Qiu, Y.; Zhu, Y.; Cao, L. Study on the Interaction between Ag and Tris(8-Hydroxyquinoline) Aluminum Using x-Ray Photoelectron Spectroscopy. *Surf. Interface Anal.* **2001**, *32*, 70–73. [[CrossRef](#)]
79. Dürr, A.C.; Koch, N.; Kelsch, M.; Rühm, A.; Ghijsen, J.; Johnson, R.; Pireaux, J.J.; Schwartz, J.; Schreiber, F.; Dosch, H.; et al. Interplay between Morphology, Structure, and Electronic Properties at Diindenoperylene-Gold Interfaces. *Phys. Rev. B* **2003**, *68*, 115428. [[CrossRef](#)]
80. Choong, V.; Park, Y.; Gao, Y.; Wehrmeister, T.; Mullen, K.; Hsieh, B.R.; Tang, C.W. Dramatic Photoluminescence Quenching of Phenylene Vinylene Oligomer Thin Films upon Submonolayer Ca Deposition. *Appl. Phys. Lett.* **1996**, *69*, 1492–1494. [[CrossRef](#)]
81. Jin, H.; Tuomikoski, M.; Hiltunen, J.; Maaninen, A.; Pino, F. Polymer-Electrode Interfacial Effect on Photovoltaic Performances in Poly(3-Hexylthiophene):Phenyl-C61-Butyric Acid Methyl Ester Based Solar Cells. *J. Phys. Chem. C* **2009**, *113*, 16807–16810. [[CrossRef](#)]
82. Jabbour, G.E.; Kawabe, Y.; Shaheen, S.E.; Wang, J.F.; Morrell, M.M.; Kippelen, B.; Peyghambarian, N. Highly Efficient and Bright Organic Electroluminescent Devices with an Aluminum Cathode. *Appl. Phys. Lett.* **1997**, *71*, 1762. [[CrossRef](#)]
83. Stöbel, M.; Staudigel, J.; Steuber, F.; Blässing, J.; Simmerer, J.; Winnacker, A.; Neuner, H.; Metzendorf, D.; Johannes, H.H.; Kowalsky, W. Electron Injection and Transport in 8-Hydroxyquinoline Aluminum. *Synth. Met.* **2000**, *111–112*, 19–24. [[CrossRef](#)]
84. Feng, X.D.; Huang, C.J.; Lui, V.; Khangura, R.S.; Lu, Z.H. Ohmic Cathode for Low-Voltage Organic Light-Emitting Diodes. *Appl. Phys. Lett.* **2005**, *86*, 143511. [[CrossRef](#)]
85. Turak, A.; Hanisch, J.; Barrena, E.; Welzel, U.; Widmaier, F.; Ahlswede, E.; Dosch, H. Systematic Analysis of Processing Parameters on the Ordering and Performance of Working Poly(3-Hexyl-Thiophene):[6,6]-Phenyl C(61)-Butyric Acid Methyl Ester Solar Cells. *J. Renew. Sustain. Energy* **2010**, *2*, 053103. [[CrossRef](#)]
86. Huang, C.J.; Grozea, D.; Turak, A.; Lu, Z.H. Passivation Effect of Al/LiF Electrode on C-60 Diodes. *Appl. Phys. Lett.* **2005**, *86*, 33107. [[CrossRef](#)]
87. Hung, L.S.; Tang, C.W.; Mason, M.G.; Raychaudhuri, P.; Madathil, J. Application of an Ultrathin LiF/Al Bilayer in Organic Surface-Emitting Diodes. *Appl. Phys. Lett.* **2001**, *78*, 544–546. [[CrossRef](#)]
88. Brabec, C.J.; Shaheen, S.E.; Winder, C.; Sariciftci, N.S.; Denk, P. Effect of LiF/Metal Electrodes on the Performance of Plastic Solar Cells. *Appl. Phys. Lett.* **2002**, *80*, 1288. [[CrossRef](#)]
89. Bory, B.F.; Rocha, P.R.F.; Janssen, R.A.J.; Gomes, H.L.; De Leeuw, D.M.; Meskers, S.C.J. Lithium Fluoride Injection Layers Can Form Quasi-Ohmic Contacts for Both Holes and Electrons. *Appl. Phys. Lett.* **2014**, *105*, 123302. [[CrossRef](#)]
90. Lu, Z.H.; Lo, C.C.; Huang, C.J.; Yuan, Y.Y.; Dharma-Wardana, M.W.C.; Zgierski, M.Z. Quasimetallic Behavior of Carrier-Polarized C60 Molecular Layers: Experiment and Theory. *Phys. Rev. B* **2005**, *72*, 155440. [[CrossRef](#)]
91. Turak, A. Cathode Interface Structure in Organic Semiconductor Devices. Ph.D. Thesis, University of Toronto, Toronto, ON, Canada, 2006.
92. Jeon, P.; Kang, S.J.; Lee, H.; Lee, J.; Jeong, K.; Lee, J.; Yi, Y. Different Contact Formations at the Interfaces of C60/LiF/Al and C60/LiF/Ag. *J. Appl. Phys.* **2012**, *111*, 073711. [[CrossRef](#)]
93. Greczynski, G.; Fahlman, M.; Salaneck, W.R. Hybrid Interfaces of Poly(9,9-Dioctylfluorene) Employing Thin Insulating Layers of CsF: A Photoelectron Spectroscopy Study. *J. Chem. Phys.* **2001**, *114*, 8628–8636. [[CrossRef](#)]
94. Salaneck, W.; Stafström, S.; Brédas, J.L. *Conjugated Polymer Surfaces and Interfaces*; Cambridge University Press: Cambridge, UK, 1996.
95. Mason, M.G.; Tang, C.W.; Hung, L.S.; Raychaudhuri, P.; Madathil, J.; Giesen, D.J.; Yan, L.; Le, Q.T.; Gao, Y.; Lee, S.T.; et al. Interfacial Chemistry of Alq<sub>3</sub> and LiF with Reactive Metals. *J. Appl. Phys.* **2001**, *89*, 2756–2765. [[CrossRef](#)]
96. Jonsson, S.K.M.; Carlegrim, E.; Zhang, F.; Salaneck, W.R.; Fahlman, M. Photoelectron Spectroscopy of the Contact between the Cathode and the Active Layers in Plastic Solar Cells: The Role of LiF. *Jpn. J. Appl. Phys. Part 1 Regul. Pap. Short Notes Rev. Pap.* **2005**, *44*, 3695–3701. [[CrossRef](#)]
97. Jönsson, S.K.M.; Salaneck, W.R.; Fahlman, M. Photoemission of Alq<sub>3</sub> and C60 Films on Al and LiF/Al Substrates. *J. Appl. Phys.* **2005**, *98*, 014901. [[CrossRef](#)]
98. Głowacki, E.D.; Marshall, K.L.; Tang, C.W.; Sariciftci, N.S. Doping of Organic Semiconductors Induced by Lithium Fluoride/Aluminum Electrodes Studied by Electron Spin Resonance and Infrared Reflection-Absorption Spectroscopy. *Appl. Phys. Lett.* **2011**, *99*, 043305. [[CrossRef](#)]

99. Hung, L.S.; Chen, C.H. Recent Progress of Molecular Organic Electroluminescent Materials and Devices. *Mat. Sci. Eng. R* **2002**, *39*, 143–222. [[CrossRef](#)]
100. Le, Q.T.; Yan, L.; Gao, Y.; Mason, M.G.; Giesen, D.J.; Tang, C.W. Photoemission Study of Aluminum/Tris-(8-Hydroxyquinoline) Aluminum and Aluminum/LiF/Tris-(8-Hydroxyquinoline) Aluminum Interfaces. *J. Appl. Phys.* **2000**, *87*, 375–379. [[CrossRef](#)]
101. Mori, T.; Fujikawa, H.; Tokito, S.; Taga, Y. Electronic Structure of 8-Hydroxyquinoline Aluminum/LiF/Al Interface for Organic Electroluminescent Device Studied by Ultraviolet Photoelectron Spectroscopy. *Appl. Phys. Lett.* **1998**, *73*, 2763–2765. [[CrossRef](#)]
102. Turak, A.; Zgierski, M.Z.; Dharma-Wardana, M.W.C. LiF Doping of C60 Studied with X-ray Photoemission Shake-Up Analysis. *ECS J. Solid State Sci. Technol.* **2017**, *6*, M3116–M3121. [[CrossRef](#)]
103. Zhao, Y.Q.; Huang, C.J.; Ogundimu, T.; Lu, Z.H. Transparent Conducting C60:LiF Nanocomposite Thin Films for Organic Light-Emitting Diodes. *Appl. Phys. Lett.* **2007**, *91*, 103109. [[CrossRef](#)]
104. Kawano, K.; Adachi, C. Reduced Initial Degradation of Bulk Heterojunction Organic Solar Cells by Incorporation of Stacked Fullerene and Lithium Fluoride Interlayers. *Appl. Phys. Lett.* **2010**, *96*, 53307. [[CrossRef](#)]
105. Lide, D.R. *CRC Handbook of Chemistry and Physics*, 90th ed.; CRC Press/Taylor and Francis: Boca Raton, FL, USA, 2010.
106. Matsumura, M.; Furukawa, K.; Jinde, Y. Effect of Al/LiF Cathodes on Emission Efficiency of Organic EL Devices. *Thin Solid Films* **1998**, *331*, 96–100. [[CrossRef](#)]
107. Hill, I.G.; Milliron, D.; Schwartz, J.; Kahn, A. Organic Semiconductor Interfaces: Electronic Structure and Transport Properties. *Appl. Surf. Sci.* **2000**, *166*, 354–362. [[CrossRef](#)]
108. Huang, M.B.; McDonald, K.; Keay, J.C.; Wang, Y.Q.; Rosenthal, S.J.; Weller, R.A.; Feldman, L.C. Suppression of Penetration of Aluminum into 8-Hydroxyquinoline Aluminum via a Thin Oxide Barrier. *Appl. Phys. Lett.* **1998**, *73*, 2914. [[CrossRef](#)]
109. Ahlswede, E.; Hanisch, J.; Powalla, M. Comparative Study of the Influence of LiF, NaF, and KF on the Performance of Polymer Bulk Heterojunction Solar Cells. *Appl. Phys. Lett.* **2007**, *90*, 163504. [[CrossRef](#)]
110. Wang, X.J.Z.J.; Zhao, J.M.; Zhou, Y.C.; Zhang, S.T.; Zhan, Y.Q.; Xu, Z.; Ding, H.J.; Zhong, G.Y.; Shi, H.Z.; Xiong, Z.H.; et al. Enhancement of Electron Injection in Organic Light-Emitting Devices Using an Ag/LiF Cathode. *J. Appl. Phys.* **2004**, *95*, 3828–3830. [[CrossRef](#)]
111. Bory, B.F.; Gomes, H.L.; Janssen, R.A.J.; de Leeuw, D.M.; Meskers, S.C.J. Electrical Conduction of LiF Interlayers in Organic Diodes. *J. Appl. Phys.* **2015**, *117*, 155502. [[CrossRef](#)]
112. Yokoyama, T.; Yoshimura, D.; Ito, E.; Ishii, H.; Ouchi, Y.; Seki, K. Energy Level Alignment at Alq<sub>3</sub>/LiF/Al Interfaces Studied by Electron Spectroscopies: Island Growth of LiF and Size-Dependence of the Electronic Structures. *Jpn. J. Appl. Phys.* **2003**, *42*, 3666. [[CrossRef](#)]
113. Montereali, R.M.; Gambino, S.; Loreti, S.; Gagliardi, S.; Pace, A.; Baldacchini, G.; Michelotti, F. Morphological, Electrical and Optical Properties of Organic Light-Emitting Diodes with a LiF/Al Cathode and an Al-Hydroxyquinoline/Diamine Junction. *Synth. Met.* **2004**, *143*, 171–174. [[CrossRef](#)]
114. Lee, Y.J.; Li, X.; Kang, D.Y.; Park, S.S.; Kim, J.; Choi, J.W.; Kim, H. Surface Morphology and Interdiffusion of LiF in Alq<sub>3</sub>-Based Organic Light-Emitting Devices. *Ultramicroscopy* **2008**, *108*, 1315–1318. [[CrossRef](#)] [[PubMed](#)]
115. Shrotriya, V.; Wu, E.; Li, G.; Yao, Y.; Yang, Y. Efficient Light Harvesting in Multiple-Device Stacked Structure for Polymer Solar Cells. *Appl. Phys. Lett.* **2006**, *88*, 064104. [[CrossRef](#)]
116. Brown, T.M.; Friend, R.H.; Millard, I.S.; Lacey, D.J.; Butler, T.; Burroughes, J.H.; Cacialli, F. Electronic Line-up in Light-Emitting Diodes with Alkali-Halide/Metal Cathodes. *J. Appl. Phys.* **2003**, *93*, 6159. [[CrossRef](#)]
117. Maye, F.; Turak, A. LiF Nanoparticles Enhance Targeted Degradation of Organic Material under Low Dose X-ray Irradiation. *Radiation* **2021**, *1*, 131–144. [[CrossRef](#)]
118. Gao, D.; Helander, M.G.; Wang, Z.B.; Puzzo, D.P.; Greiner, M.T.; Lu, Z.H. C60:LiF Blocking Layer for Environmentally Stable Bulk Heterojunction Solar Cells. *Adv. Mater.* **2010**, *22*, 5404–5408. [[CrossRef](#)]
119. Chin, B.D.; Duan, L.; Kim, M.H.; Lee, S.T.; Chung, H.K. Effects of Cathode Thickness and Thermal Treatment on the Design of Balanced Blue Light-Emitting Polymer Device. *Appl. Phys. Lett.* **2004**, *85*, 4496–4498. [[CrossRef](#)]
120. Ganzorig, C.; Fujihira, M. A Lithium Carboxylate Ultrathin Film on an Aluminum Cathode for Enhanced Electron Injection in Organic Electroluminescent Devices. *Jpn. J. Appl. Phys. Part 2 Lett.* **1999**, *38*, L1348–L1350. [[CrossRef](#)]
121. Kawano, K.; Pacios, R.; Poplavskyy, D.; Nelson, J.; Bradley, D.D.C.; Durrant, J.R. Degradation of Organic Solar Cells Due to Air Exposure. *Sol. Energy Mat. Sol. Cells* **2006**, *90*, 3520–3530. [[CrossRef](#)]
122. Krebs, F.C.; Carle, J.E.; Cruys-Bagger, N.; Andersen, M.; Lilledal, M.R.; Hammond, M.A.; Hvidt, S. Lifetimes of Organic Photovoltaics: Photochemistry, Atmosphere Effects and Barrier Layers in ITO-MEHPPV:PCBM-Aluminium Devices. *Sol. Energy Mater. Sol. Cells* **2005**, *86*, 499–516. [[CrossRef](#)]
123. Lattante, S.; Perulli, A.; Anni, M. Study of the Series Resistance Evolution in Organic Solar Cells by Use of the Lambert W Function. *Synth. Met.* **2011**, *161*, 949–952. [[CrossRef](#)]
124. Sato, Y.; Ogata, T.; Ichinosawa, S.; Fugono, M.; Kanai, H. Interface and Material Considerations of OLEDs. *Proc. SPIE* **1999**, *3797*, 198–208. [[CrossRef](#)]
125. Wang, M.D.; Xie, F.Y.; Xie, W.G.; Zheng, S.Z.; Ke, N.; Chen, J.; Zhao, N.; Xu, J.B. Device Lifetime Improvement of Polymer-Based Bulk Heterojunction Solar Cells by Incorporating Copper Oxide Layer at Al Cathode. *Appl. Phys. Lett.* **2011**, *98*, 183304. [[CrossRef](#)]

126. Yi, Y.J.; Kang, S.J.; Cho, K.; Koo, J.M.; Han, K.; Park, K.; Noh, M.; Whang, C.N.; Jeong, K. Origin of the Improved Luminance-Voltage Characteristics and Stability in Organic Light-Emitting Device Using CsCl Electron Injection Layer. *Appl. Phys. Lett.* **2005**, *86*, 213502. [[CrossRef](#)]
127. Rocha, P.R.; Gomes, H.L.; Asadi, K.; Katsouras, I.; Bory, B.; Verbakel, F.; van de Weijer, P.; de Leeuw, D.M.; Meskers, S.C. Sudden Death of Organic Light-Emitting Diodes. *Org. Electron.* **2015**, *20*, 89–96. [[CrossRef](#)]
128. Paci, B.; Generosi, A.; Albertini, V.R.; Perfetti, P.; de Bettignies, R.; Leroy, J.; Firon, M.; Senten, C. Controlling Photoinduced Degradation in Plastic Photovoltaic Cells: A Time-Resolved Energy Dispersive x-Ray Reflectometry Study. *Appl. Phys. Lett.* **2006**, *89*, 43507. [[CrossRef](#)]
129. Choong, V.E.; Shi, S.; Curless, J.; So, F. Bipolar Transport Organic Light Emitting Diodes with Enhanced Reliability by LiF Doping. *Appl. Phys. Lett.* **2000**, *76*, 958–960. [[CrossRef](#)]
130. Ghorashi, S.M.B.; Behjat, A.; Ajeian, R. The Effect of a Buffer Layer on the Performance and Optimal Encapsulation Time of ITO/CuPc/C(60)/Buffer/Cu Bilayer Cells. *Sol. Energy Mater. Sol. Cells* **2012**, *96*, 50–57. [[CrossRef](#)]
131. Jung, G.Y.; Yates, A.; Samuel, I.D.W.; Petty, M.C. Lifetime Studies of Light-Emitting Diode Structures Incorporating Polymeric Langmuir–Blodgett Films. *Mater. Sci. Eng. C* **2001**, *14*, 1–10. [[CrossRef](#)]
132. Huang, J.J.; Su, Y.K.; Chang, M.H.; Hsieh, T.E.; Huang, B.R.; Wang, S.H.; Chen, W.R.; Tsai, Y.S.; Hsieh, H.E.; Liu, M.O.; et al. Lifetime Improvement of Organic Light Emitting Diodes Using LiF Thin Film and UV Glue Encapsulation. *Jpn. J. Appl. Phys.* **2008**, *47*, 5676–5680. [[CrossRef](#)]
133. Konenkamp, R.; Priebe, G.; Pietzak, B. Carrier Mobilities and Influence of Oxygen in C60 Films. *Phys. Rev. B* **1999**, *60*, 11804–11808. [[CrossRef](#)]
134. Tanaka, Y.; Kanai, K.; Ouchi, Y.; Seki, K. Oxygen Effect on the Interfacial Electronic Structure of C60 Film Studied by Ultraviolet Photoelectron Spectroscopy. *Chem. Phys. Lett.* **2007**, *441*, 63–67. [[CrossRef](#)]
135. Pevzner, B.; Hebard, A.F.; Dresselhaus, M.S. Role of Molecular Oxygen and Other Impurities in the Electrical Transport and Dielectric Properties of C-60 Films. *Phys. Rev. B* **1997**, *55*, 16439–16449. [[CrossRef](#)]
136. Zur, A.; McGill, T.C. Lattice Match: An Application to Heteroepitaxy. *J. Appl. Phys.* **1984**, *55*, 378–386. [[CrossRef](#)]
137. Pearson, W.B. *A Handbook of Lattice Spacings and Structures of Metals and Alloys*; Pergamon Press: Oxford, UK, 1967.
138. Euwema, R.N.; Wepfer, G.G.; Surratt, G.T.; Wilhite, D.L. Hartree-Fock Calculations for Crystalline Ne and LiF. *Phys. Rev. B* **1974**, *9*, 5249–5256. [[CrossRef](#)]
139. Kumari, L.; Li, W.Z.; Vannoy, C.H.; Leblanc, R.M.; Wang, D.Z. Synthesis, Characterization and Optical Properties of Mg(OH)<sub>2</sub> Micro-/Nanostructure and Its Conversion to MgO. *Ceram. Int.* **2009**, *35*, 3355–3364. [[CrossRef](#)]
140. Hagino, Y. Studies on Basic Magnesium Carbonate (Part IX). *Bull. Soc. Salt Sci. Jpn.* **1956**, *10*, 77–82. [[CrossRef](#)]
141. Cabrera, N.; Mott, N.F. Theory of the Oxidation of Metals. *Rep. Prog. Phys.* **1949**, *12*, 163–184. [[CrossRef](#)]
142. Keski-Kuha, R.; Larruquert, J.; Gum, J.; Fleetwood, C. *Optical Coatings and Materials for Ultraviolet Space Applications*; ASP Conference; Astronomical Society of the Pacific: Boulder, CO, USA, 1999; Volume 164, p. 406.
143. Liu, F.; Ruden, P.P.; Campbell, I.H.; Smith, D.L. Electrostatic Capacitance in Single and Double Layer Organic Diodes. *Appl. Phys. Lett.* **2012**, *101*, 023501. [[CrossRef](#)]
144. Sohn, S.; Park, K.; Lee, D.; Jung, D.; Kim, H.M.; Manna, U.; Yi, J.; Boo, J.H.; Chae, H.; Kim, H. Characteristics of Polymer Light Emitting Diodes with the LiF Anode Interfacial Layer. *Jpn. J. Appl. Phys.* **2006**, *45*, 3733–3736. [[CrossRef](#)]
145. Niu, L.; Guan, Y. Which Is Better as a Buffer Layer for Organic Light-Emitting Devices, CsF or LiF? *Phys. Status Solidi A* **2010**, *207*, 993–997. [[CrossRef](#)]
146. Zhao, Y.; Liu, S.Y.; Hou, J.Y. Effect of LiF Buffer Layer on the Performance of Organic Electroluminescent Devices. *Thin Solid Films* **2001**, *397*, 208–210. [[CrossRef](#)]
147. Li, W.; Song, Q.; Sun, X.; Wang, M.; Wu, H.; Ding, X.; Hou, X. Interfacial Processes in Small Molecule Organic Solar Cells. *Sci. China Phys. Mech. Astron.* **2010**, *53*, 288–300. [[CrossRef](#)]
148. Song, Q.L.; Wu, H.R.; Ding, X.M.; Hou, X.Y.; Li, F.Y.; Zhou, Z.G. Exciton Dissociation at the Indium Tin Oxide-N,N'-Bis(Naphthalen-1-Yl)-N,N'-Bis(Phenyl) Benzidine Interface: A Transient Photovoltage Study. *Appl. Phys. Lett.* **2006**, *88*, 232101. [[CrossRef](#)]
149. Sun, X.Y.; Song, Q.L.; Wang, M.L.; Ding, X.M.; Hou, X.Y.; Zhou, Z.G.; Li, F.Y. The Dissociation of Excitons at Indium Tin Oxide-Copper Phthalocyanine Interface in Organic Solar Cells. *J. Appl. Phys.* **2008**, *104*, 103702. [[CrossRef](#)]
150. Zhao, J.M.; Zhang, S.T.; Wang, X.J.; Zhan, Y.Q.; Wang, X.Z.; Zhong, G.Y.; Wang, Z.J.; Ding, X.M.; Huang, W.; et al. Dual Role of LiF as a Hole-Injection Buffer in Organic Light-Emitting Diodes. *Appl. Phys. Lett.* **2004**, *84*, 2913. [[CrossRef](#)]
151. Lee, S.N.; Hsu, S.F.; Hwang, S.W.; Chen, C.H. Effects of Substrate Treatment on the Electroluminescence Performance of Flexible OLEDs. *Curr. Appl. Phys.* **2004**, *4*, 651–654. [[CrossRef](#)]
152. Zhu, F.R.; Low, B.L.; Zhang, K.R.; Chua, S.J. Lithium-Fluoride-Modified Indium Tin Oxide Anode for Enhanced Carrier Injection in Phenyl-Substituted Polymer Electroluminescent Devices. *Appl. Phys. Lett.* **2001**, *79*, 1205–1207. [[CrossRef](#)]
153. Kurt, H.; Jia, J.; Shigesato, Y.; Ow-Yang, C.W. Tuning Hole Charge Collection Efficiency in Polymer Photovoltaics by Optimizing the Work Function of Indium Tin Oxide Electrodes with Solution-Processed LiF Nanoparticles. *J. Mater. Sci. Mater. Electron.* **2015**, *26*, 9205–9212. [[CrossRef](#)]
154. Kim, H.S.; Lee, H.; Jeon, P.E.; Jeong, K.; Lee, J.H.; Yi, Y. Revised Hole Injection Mechanism of a Thin LiF Layer Introduced between Pentacene and an Indium Tin Oxide Anode. *J. Appl. Phys.* **2010**, *108*, 053701. [[CrossRef](#)]

155. Xiao, T.; Cui, W.; Cai, M.; Liu, R.; Anderegg, J.W.; Shinar, J.; Shinar, R. Thin Air-Plasma-Treated Alkali Fluoride Layers for Improved Hole Extraction in Copper Phthalocyanine/C70-Based Solar Cells. *JPE JPEOBV* **2012**, *2*, 021006. [[CrossRef](#)]
156. Grozea, D.; Turak, A.; Yuan, Y.; Han, S.; Lu, Z.H.; Kim, W.Y. Enhanced Thermal Stability in Organic Light-Emitting Diodes through Nanocomposite Buffer Layers at the Anode/Organic Interface. *J. Appl. Phys.* **2007**, *101*, 033522. [[CrossRef](#)]
157. Heidkamp, J.; Maye, F.; Turak, A.Z. Stabilization Methods for Small Molecule Dewetting on Indium Tin Oxide Substrates for Organic Photovoltaics. In *Proceeding of SPIE*; Cheben, P., Schmid, J., Boudoux, C., Chen, L.R., Delâge, A., Janz, S., Kashyap, R., Lockwood, D.J., Looock, H.P., Mi, Z., Eds.; SPIE: Ottawa, ON, Canada, 2013; Volume 8915, p. 891508. [[CrossRef](#)]
158. Sharma, S.; Rafailovich, M.H.; Peiffer, D.; Sokolov, J. Control of Dewetting Dynamics by Adding Nanoparticle Fillers. *Nano Lett.* **2001**, *1*, 511–514. [[CrossRef](#)]
159. Barnes, K.A.; Karim, A.; Douglas, J.F.; Nakatani, A.I.; Gruell, H.; Amis, E.J. Suppression of Dewetting in Nanoparticle-Filled Polymer Films. *Macromolecules* **2000**, *33*, 4177–4185. [[CrossRef](#)]
160. Mukherjee, R.; Das, S.; Das, A.; Sharma, S.K.; Raychaudhuri, A.K.; Sharma, A. Stability and Dewetting of Metal Nanoparticle Filled Thin Polymer Films: Control of Instability Length Scale and Dynamics. *ACS Nano* **2010**, *4*, 3709–3724. [[CrossRef](#)]